Structural Change of the Mn Cluster during the $S_2 \rightarrow S_3$ State Transition of the Oxygen-Evolving Complex of Photosystem II. Does It Reflect the Onset of Water/Substrate Oxidation? Determination by Mn X-ray Absorption Spectroscopy

Wenchuan Liang,*,‡,§,† Theo A. Roelofs,‡,|| Roehl M. Cinco,‡,§ Annette Rompel,‡,¶ Matthew J. Latimer,‡,§,# Wa O. Yu,‡,⊥ Kenneth Sauer,*,‡,§ Melvin P. Klein,*,‡ and Vittal K. Yachandra*,‡

Contribution from the Melvin Calvin Laboratory, Physical Biosciences Division, Lawrence Berkeley National Laboratory, and Department of Chemistry, University of California, Berkeley, California 94720-5230

Received July 15, 1999

Abstract: The oxygen-evolving complex of Photosystem II in plants and cyanobacteria catalyzes the oxidation of two water molecules to one molecule of dioxygen. A tetranuclear Mn complex is believed to cycle through five intermediate states (S_0–S_4) to couple the four-electron oxidation of water with the one-electron photochemistry occurring at the Photosystem II reaction center. We have used X-ray absorption spectroscopy to study the local structure of the Mn complex and have proposed a model for it, based on studies of the Mn K-edges and the extended X-ray absorption fine structure of the S_1 and S_2 states. The proposed model consists of two di-μ-oxo-bridged binuclear Mn units with Mn−Mn distances of ∼2.7 Å that are linked to each other by a mono-μ-oxo bridge with a Mn−Mn separation of ∼3.3 Å. The Mn−Mn distances are invariant in the native S_1 and S_2 states. This report describes the application of X-ray absorption spectroscopy to S_3 samples created under physiological conditions with saturating flash illumination. Significant changes are observed in the Mn−Mn distances in the S_3 state compared to the S_1 and the S_2 states. The two 2.7 Å Mn−Mn distances that characterize the di-μ-oxo centers in the S_1 and S_2 states are lengthened to ∼2.8 and 3.0 Å in the S_3 state, respectively. The 3.3 Å Mn−Mn and Mn−Ca distances also increase by 0.04−0.2 Å. These changes in Mn−Mn distances are interpreted as consequences of the onset of substrate/water oxidation in the S_3 state. Mn-centered oxidation is evident during the $S_0 \rightarrow S_1$ and $S_1 \rightarrow S_2$ transitions. We propose that the changes in Mn−Mn distances during the $S_2 \rightarrow S_3$ transition are the result of ligand or water oxidation, leading to the formation of an oxyl radical intermediate formed at a bridging or terminal position. The reaction of the oxyl radical with OH^-, H_2O, or an oxo group during the subsequent S state conversion is proposed to lead to the formation of the O−O bond. Models that can account for changes in the Mn−Mn distances in the S_3 state and the implications for the mechanism of water oxidation are discussed.

Introduction

The oxidation of water to dioxygen in plants and cyanobacteria involves the stepwise transfer of oxidizing equivalents by the Photosystem II (PS II)[1] reaction center to the quinone electron acceptors. Photon absorption at PS II results in the transfer of electrons sequentially until four electrons are removed from two water molecules to produce one molecule of dioxygen. The oxidizing potential produced by photosynthetic charge separation at PS II is thought to accumulate at a site in the membrane-bound proteins denoted the oxygen-evolving complex (OEC).[2–5] A tetranuclear Mn complex in the OEC is believed

to cycle through five intermediate states S_i ($i = 0$–4), with i representing the number of oxidative equivalents accumulated in the OEC.[6] After long-term dark adaptation (tens of minutes), nearly all of the PS II centers are present at the S_1 state. The postulated S_4 state is a transient intermediate that spontaneously returns to the S_0 state with the release of dioxygen.

Investigation of the structure of the Mn complex at each S state is essential for understanding the catalytic mechanism of photosynthetic oxygen evolution. We have used X-ray absorp-

* To whom correspondence should be addressed. Tel.: (510) 486 4331. Fax: (510) 486 6059. E-mail: vkyachandra@lbl.gov or khsauer@lbl.gov or mpklein@lbl.gov.

‡ Physical Biosciences Division, Lawrence Berkeley National Laboratory.

§ Department of Chemistry, University of California, Berkeley.

† Present address: B400, Department of Biochemistry, School of Medicine, Stanford University, Stanford, CA 94305-5307.

|| Present address: Robert-Rössle-Clinic, University Hospital Charité, D-13122 Berlin, Germany.

Present address: Stanford Synchrotron Radiation Laboratory, Stanford University, Stanford, CA 94305.

¶ Present address: Westfälische Wilhelms-Universität, Münster, Germany.

⊥ Present address: Department of Molecular and Cell Biology, University of California, Berkeley, CA 94720.

(1) Abbreviations: Chl, chlorophyll; EPR, electron paramagnetic resonance; EXAFS, extended X-ray absorption fine structure; ESEEM, electron spin-echo envelope modulation; FT, Fourier transform; MES, 2-[N-morpholino]ethanesulfonic acid; MLS, multiline EPR signal; OEC, oxygen-evolving complex; PPBQ, phenyl-*p*-benzoquinone; PS II, photosystem II; Y_D^{ox}, oxidized tyrosine D; $Y_Z^•$, oxidized tyrosine Z residue; XANES, X-ray absorption near-edge structure; XAS, X-ray absorption spectroscopy.

(2) Debus, R. J. *Biochim. Biophys. Acta* **1992**, *1102*, 269−352.

(3) Rutherford, A. W.; Zimmermann, J.-L.; Boussac, A. In *The Photosystems: Structure, Function, and Molecular Biology*; Barber, J., Ed.; Elsevier B.V.: Amsterdam, 1992; pp 179−229.

(4) Britt, R. D. In *Oxygenic Photosynthesis: The Light Reactions*; Ort, D. R., Yocum, C. F., Eds.; Kluwer Academic Publishers: Dordrecht, 1996; pp 137−164.

(5) Yachandra, V. K.; Sauer, K.; Klein, M. P. *Chem. Rev.* **1996**, *96*, 2927−2950.

(6) Kok, B.; Forbush, B.; McGloin, M. *Photochem. Photobiol.* **1970**, *11*, 457−476.

tion spectroscopy (XAS) in conjunction with electron paramagnetic resonance spectroscopy (EPR) to study the oxidation state(s) and structural changes in the Mn complex as the OEC advances through the S state cycle.[5] XAS is a convenient technique for studying the structure of the Mn complex from PS II preparations that are prepared in the various S states and frozen as solutions. The energy of the incoming X-ray beam and of the outgoing fluorescence is specific to the Mn atom; hence, other metals or the protein matrix normally copurified with the OEC in a PS II preparation do not interfere. X-ray absorption near-edge structure (XANES) is sensitive to both the oxidation state and the symmetry of the Mn cluster. Extended X-ray absorption fine structure (EXAFS) provides information about the types, numbers, and distances of the neighboring backscattering atoms from the absorbing Mn atoms.[7−9]

We have proposed a "dimer-of-dimers" model for the structure of the Mn cluster based on studies of the Mn K-edges and the extended X-ray absorption fine structure (EXAFS) of the S_1 and S_2 states.[10] This model represents one of the simplest explanations of the EXAFS data but is not unique.[5,11,15] The Mn cluster is proposed to consist of two di-μ-oxo-bridged Mn−Mn binuclear units which are linked to each other by a mono-μ-oxo-bridging ligand. The Mn−Mn distance is ∼2.7 Å within each of the di-μ-oxo units, and is ∼3.3 Å when the Mn atoms are linked by the mono-μ-oxo-bridging ligand.

XAS experiments on the S_3 and S_0 states have been difficult for the PS II samples generated by single flashes. The requirement of optically dilute samples to ensure saturation by single actinic flashes generally results in a low signal-to-noise ratio of the Mn X-ray fluorescence. To explore the structures beyond the S_2 state, X-ray absorption spectra have been collected on chemically treated S_3 and S_0 states accumulated by continuous illumination at cryogenic temperatures.[12,13] Reduced derivatives of the Mn cluster prepared by treatment with NH_2OH or hydroquinone have also been investigated using XAS methods.[14,15] Recently, we have been able to collect a series of Mn K-edge and EXAFS data from flash-induced samples prepared under physiological conditions. Furthermore, pure S state XANES spectra of high quality were extracted from linear combinations of the flash-induced XAS spectra.[16] Each of the $S_0{\rightarrow}S_1$ and $S_1{\rightarrow}S_2$ transitions is accompanied by a shift of the edge to higher energies, indicating that during those transitions the Mn cluster undergoes oxidation. The $S_2{\rightarrow}S_3$ transition, however, results in a very small edge shift, consistent with the absence of a direct Mn oxidation step. This suggests that the observed edge shift during the $S_2{\rightarrow}S_3$ transition may be attributed to ligand/substrate oxidation of the Mn cluster rather than to direct Mn oxidation. However, on the basis of Mn

K-edge studies, other groups have proposed that Mn is oxidized during the $S_0{\rightarrow}S_1$, $S_1{\rightarrow}S_2$, and also during the $S_2{\rightarrow}S_3$ transitions.[17,18]

The requirement of a higher signal-to-noise ratio for the EXAFS relative to the XANES experiments has made EXAFS measurements more difficult for the flash-induced S state samples. Earlier EXAFS data from the chemically treated S_3 state samples produced by a double-turnover method indicated that the two di-μ-oxo-bridged Mn−Mn dimer units may become nonequivalent.[12] The EXAFS spectra from calcium-depleted $S_3{}'$ samples ($S_2Y_Z{}^{\bullet}$) prepared by low-pH treatment in a citrate buffer do not exhibit similar heterogeneity in the 2.7 Å Mn−Mn distances.[19,20] However, when NaCl treatment is used for Ca depletion, Evans and co-workers have shown that the 2.7 Å Fourier feature attributed to Mn−Mn interaction is split into 2.7 and 3.0 Å features that are most apparent in the $S_3{}'$ state.[21] We have previously reported preliminary Fourier transforms of the S_3 state samples prepared under physiological conditions with saturating flashes.[19] Since then, data have been collected and analyzed on more samples. In this report we present a detailed analysis of the structural changes observed for the S_3 state and the implications for the mechanism of water oxidation.

Material and Methods

Preparation of PS II-Enriched Membranes. PS II-enriched membranes were prepared from spinach by a modified BBY protocol.[22] The incubation time for detergent treatment was 1 min. The pelleted PS II-enriched membranes were washed in medium A (15 mM NaCl, 5 mM $MgCl_2$, 5 mM $CaCl_2$, and 50 mM MES at pH 6.5) with 0.4 M sucrose and centrifuged for 30 min at 37000g. After one more wash and centrifugation at 37000g for 30 min, pelleted PS II was resuspended into medium A with 50% (v/v) glycerol to a Chl concentration of 4−5 mg/mL. Typical oxygen evolution activities were 400−550 μmol of O_2 mg^{-1} of Chl h^{-1}.

A freshly prepared stock solution (50 mM in dimethyl sulfoxide) of phenyl-p-benzoquinone (PPBQ) was added to the PS II samples to a final concentration of 500 μM just before flash illumination. PPBQ (Eastman Kodak) was recrystallized from ethanol. PS II membrane suspensions were loaded directly into Lucite sample holders with inner dimensions of 18 × 2.5 × 0.8 mm. All of the flash illuminations, EPR, and X-ray absorption measurements were performed directly on samples mounted in these holders. The samples were dark-adapted for at least 1 h at 4 °C before being frozen to 77 K in liquid nitrogen. The amplitude of the $Y_D{}^{ox}$ EPR signal was measured and used to correct for sample volume fluctuations. The samples were then equilibrated to room temperature (22−24 °C) in the dark for at least 20 min before the flash illumination procedure was applied.

Oxygen Evolution Measurements. Oxygen evolution activity was measured by using a Clark-type oxygen electrode (Yellow Springs Instruments, Yellow Springs, OH) as described by DeRose.[23] A 5% $CuSO_4$ solution in a spherical flask was used to focus the light onto the cuvette and to serve as a heat filter.

Flash-Induced Illuminations of PS II. The source was either a Xe flash lamp (CHH 174, ILC Inc.) which generated flashes of white light

(7) Scott, R. A. *Methods Enzymol.* **1985**, *117*, 414−459.

(8) Cramer, S. P. In *X-ray Absorption: Principles, Applications and Techniques of EXAFS, SEXAFS, and XANES*; Koningsberger, D. C., Prins, R., Eds.; Wiley-Interscience: New York, 1988; pp 257−320.

(9) Yachandra, V. K. *Methods Enzymol.* **1995**, *246*, 638−675.

(10) Yachandra, V. K.; DeRose, V. J.; Latimer, M. J.; Mukerji, I.; Sauer, K.; Klein, M. P. *Science* **1993**, *260*, 675−679.

(11) DeRose, V. J.; Mukerji, I.; Latimer, M. J.; Yachandra, V. K.; Sauer, K.; Klein, M. P. *J. Am. Chem. Soc.* **1994**, *116*, 5239−5249.

(12) Guiles, R. D.; Zimmermann, J.-L.; McDermott, A. E.; Yachandra, V. K.; Cole, J. L.; Dexheimer, S. L.; Britt, R. D.; Wieghardt, K.; Bossek, U.; Sauer, K.; Klein, M. P. *Biochemistry* **1990**, *29*, 471−485.

(13) Guiles, R. D.; Yachandra, V. K.; McDermott, A. E.; Cole, J. L.; Dexheimer, S. L.; Britt, R. D.; Sauer, K.; Klein, M. P. *Biochemistry* **1990**, *29*, 486-496.

(14) Riggs-Gelasco, P. J.; Mei, R.; Yocum, C. F.; Penner-Hahn, J. E. *J. Am. Chem. Soc.* **1996**, *118*, 2387−2399.

(15) Penner-Hahn, J. E. *Struct. Bonding* **1998**, *90*, 1−36.

(16) Roelofs, T. A.; Liang, W.; Latimer, M. J.; Cinco, R. M.; Rompel, A.; Andrews, J. C.; Sauer, K.; Yachandra, V. K.; Klein, M. P. *Proc. Natl. Acad. Sci. U.S.A.* **1996**, *93*, 3335−3340.

(17) Ono, T.-A.; Noguchi, T.; Inoue, Y.; Kusunoki, M.; Matsushita, T.; Oyanagi, H. *Science* **1992**, *258*, 1335−1337.

(18) Iuzzolino, L.; Dittmer, J.; Dörner, W.; Meyer-Klaucke, W.; Dau, H. *Biochemistry* **1998**, *37*, 17112−17119.

(19) Liang, W.; Roelofs, T. A.; Olsen, G. T.; Latimer, M. J.; Cinco, R. M.; Rompel, A.; Sauer, K.; Yachandra, V. K.; Klein, M. P. In *Photosynthesis: From Light to Biosphere*; Mathis, P., Ed.; Kluwer: Dordrecht, 1995; Vol. II, pp 413−416.

(20) Latimer, M. J.; DeRose, V. J.; Yachandra, V. K.; Sauer, K.; Klein, M. P. *J. Phys. Chem. B* **1998**, *102*, 8257−8265.

(21) MacLachlan, D. J.; Nugent, J. H. A.; Bratt, P. J.; Evans, M. C. W. *Biochim. Biophys. Acta* **1994**, *1186*, 186−200.

(22) Berthold, D. A.; Babcock, G. T.; Yocum, C. F. *FEBS Lett.* **1981**, *134*, 231−234.

(23) DeRose, V. J. Lawrence Berkeley Laboratory Report LBL-30077 Thesis, University of California, Berkeley, 1990.

of 14 μs full-width at half-maximum (fwhm), or a frequency-doubled (532 nm) Nd:YAG laser of 8 ns fwhm. To maintain maximal synchronization of the PS II centers upon flash illumination, fast recombination reactions between both the S_2 and S_3 states and the reduced form of the redox-active tyrosine residue Y_D must be suppressed. This was achieved by the application of two preflashes, followed by a 60-min dark adaptation period at room temperature. This procedure synchronizes almost all PS II centers into the $S_1Y_D^{ox}$ state. Each sample was next given 0, 1, 2, 3, 4, or 5 flashes, at room temperature, with 1.5 s intervals between individual flashes. The light was directed to the samples by a light guide when the Xe flash lamp was used for illumination, or focused using cylindrical lenses when the YAG laser was employed. After the last flash, the samples were frozen immediately (within 1 s) in liquid nitrogen. The EPR spectra (both Y_D^{ox} and the MLS) were collected, and the samples were stored at 77 K for further use in the XAS experiments (within 7−10 days).

Light saturation of the PS II samples was ensured in two ways. First, the S_2 state MLS amplitude induced by one flash was compared with that of an identical sample subjected to a low-temperature continuous illumination (10 min at 190 K) commonly used to generate a maximal S_2 state MLS. These amplitudes were indistinguishable within the accuracy of the MLS amplitude determination. We additionally determined the flash-intensity dependence of the MLS amplitude for a single flash. When only 60% of the maximal flash intensity was used, the MLS was 95% of the maximal amplitude. Reducing the energy to 25% resulted in 80% of the maximum MLS. Both observations indicate that the full-intensity flashes were nearly saturating, so that a reasonably small value for the miss parameter can be expected.

EPR Measurements. Low-temperature X-band EPR spectra were recorded using a Varian E109 EPR spectrometer equipped with a model 102 microwave bridge. For the MLS measurement, the sample temperature was maintained at 8 K using an Air Products LTR liquid helium cryostat. Spectrometer conditions were as follows: microwave frequency, 9.21 GHz; field modulation amplitude, 3.2 mT at 100 kHz; microwave power, 11 mW. EPR MLS amplitudes were quantitated by adding peak-to-trough amplitudes of three of the downfield and three of the upfield hyperfine lines, relative to $g = 2$. Sample temperature was kept at 18 K for the measurements of the Y_D^{ox} signal, with the following spectrometer conditions: microwave frequency, 9.21 GHz; field modulation amplitude, 3.2 mT at 100 kHz; microwave power, 0.5 μW. The field modulation amplitude of 3.2 mT gives rise to a modulation-broadened Y_D^{ox} signal that is easily quantitated. After the XAS experiments the EPR spectra of the samples were remeasured to ascertain the possible damage induced by the intense X-ray beam. The amplitude of the MLS was typically ≥80% relative to that measured before the X-ray exposure. In addition, no free Mn^{2+} EPR signal was detected in any of these samples. This indicated that no significant radiation damage occurred during the data collection.

X-ray Absorption Measurements. The manganese EXAFS spectra were collected at the beamlines 7-3, 4-2, 6-2, and 10-2 at the Stanford Synchrotron Radiation Laboratory (SSRL) (SPEAR operating at 40−100 mA at 3.0 GeV); some data were collected at the bending magnet beamline X-9B at the National Synchrotron Light Source (NSLS) (100−250 mA at 2.5 GeV). An unfocused X-ray beam was used on 7-3 at SSRL and at X9B at NSLS, while a focused beam was used for measurements at 4-2, 6-2, and 10-2 at SSRL. A Si ⟨220⟩ double-crystal monochromator was used, with the second crystal detuned to 50% of the maximum flux to reduce the transmission of the harmonics. The sample was maintained at 10 ± 1 K in a liquid helium cryostat (Oxford Instruments, CF1204). A 13-element Ge solid-state detector (Canberra Instruments) was used[24] to detect the Mn fluorescence signal.[25] We set different SCA windows for the each of the three concentric circles of detector elements, with shaping times of 1, 0.75, and 0.5 μs, based on the total number of counts each channel detects. The shaping time for the center channel, which "sees" the fewest total counts, is set at 1.0 μs, and for the outer channels that detect more total counts, because of increased scatter, the shaping time was set at 0.5 μs. This kind of

attention to detail is necessary for collecting data from these dilute samples with good S/N ratios. The total number of fluorescence counts in the SCAs above the Mn K-edge (at 6600 eV) is ∼2000/s from the dilute samples, compared to ∼10000/s for the more concentrated samples. The dilute samples were 5−6 mg of Chl/ml, whereas the concentrated samples are estimated to be 25−30 mg of Chl/ml.

EXAFS spectra were recorded from 6500 to 7100 eV, with higher point density around the pre-edge region for better KMnO₄ energy referencing. Typically, 25−40 scans of about 20 min each were collected and averaged for each S_3 spectrum. The Mn K-edge was monitored closely to detect any photoreduction. Energy calibration and resolution were monitored by simultaneously measuring the absorption spectrum of KMnO₄, using its narrow pre-edge "white-line" at 6543.30 eV. The X-ray photon flux on the samples was kept below a maximum flux density of 7×10^8 photons s^{-1} mm^{-2} of PS II sample. We have examined the effect on the various S states, and this is the maximum photon density, in the energy region between 6500 and 7100 eV, that one can safely use, within the conditions of temperature, pressure, and cryo-protectant concentration as described above.

EXAFS Data Analysis. EXAFS data were analyzed as reported previously.[11,26] A brief outline follows. The EXAFS modulation of the absorption $\chi(k)$ is described by the equation

$$\chi(k) = S_0^2 \sum_i N_i B_i(k) \frac{f_{\text{eff}}(\pi,k,R_i)}{kR_i^2} \exp(-2\sigma^2 k^2) \exp\left(\frac{-2R_i}{\lambda(k)}\right) \times$$
$$\sin[2kR_i + 2\delta_i^c(k) + \phi_i(k)] \quad (1)$$

where for each shell i, N_i is the number of scatterers at a distance R_i, S_0^2 is the many-body amplitude reduction factor, $B_i(k)$ is an amplitude reduction factor caused by inelastic forces in the central atom, f_{eff} is the effective backscattering amplitude of the scattering atom, δ_i^c and ϕ_i are the phase shifts for the absorber and backscatterer, respectively, σ^2 is the Debye−Waller term describes the attenuating effect resulting from thermal and static disorder, and $\lambda(k)$ is the mean free-path of the photoelectron. The basic structure used for calculation of FEFF5.05 fitting functions ($f_{\text{eff}}, \delta, \phi, \lambda$) was a di-$\mu$-oxo-bridged binuclear structure linked to a similar moiety by a mono-μ-oxo bridge. k is the magnitude of the photoelectron wave vector given by $k = (2\pi/h)[2m_e(E - E_0)]^{1/2}$, where m_e is the electron mass, E is the X-ray photon energy, E_0 is the threshold photoionization energy, and h is Planck's constant. All spectra were weighted by k^3, and Fourier transforms were obtained from k-space spectra in the range of ∼3.5−11.5 Å^{-1}. A three- or four-domain cubic spline was applied to the k^3-weighted data to minimize background contributions. For some data sets, a two-domain spline was applied in energy space to remove the background contribution. For such data sets, no further background removal was applied to the k-space data. A window function was applied to isolate Fourier peaks individually and in pairs to minimize the distorting effects due to Fourier isolation. These isolated Fourier peak(s) were back-transformed into k-space data and used for curve fitting. Further details of the EXAFS analysis have been reported previously.[20,23,27]

The Fourier isolates were fit with theoretical values for the backscattering amplitude and phase shifts for the scattering−absorbing pairs, based on values calculated using the FEFF5.05 program.[28−30] Details of parameters using the FEFF5.05 program have been reported previously.[26] Coordination numbers N_i are calculated on a per Mn basis and are interpreted here in the context of a total of four Mn atoms per PS II. This means that a single Mn−scatterer interaction in the complex would result in a coordination number of 0.25. More scatterers would appear in multiples of 0.25. However, in the case of Mn−Mn interactions, one Mn−Mn interaction would give a minimum coordina-

(24) Cramer, S. P.; Tench, O.; Yocum, M.; George, G. N. *Nuclear Instrum. Methods Phys. Res.* **1988**, *A266*, 586−591.

(25) Jaklevic, J.; Kirby, J. A.; Klein, M. P.; Robertson, A. S.; Brown, G.; Eisenberger, P. *Solid State Commun.* **1977**, *23*, 679−682.

(26) Latimer, M. J.; DeRose, V. J.; Mukerji, I.; Yachandra, V. K.; Sauer, K.; Klein, M. P. *Biochemistry* **1995**, *34*, 10898−10909.

(27) Guiles, R. D. Lawrence Berkeley Laboratory Report LBL-25186 Thesis, University of California, Berkeley, 1988.

(28) Rehr, J. J.; Mustre de Leon, J.; Zabinsky, S. I.; Albers, R. C. *J. Am. Chem. Soc.* **1991**, *113*, 5135−5140.

(29) Rehr, J. J.; Albers, R. C.; Zabinsky, S. I. *Phys. Rev. Lett.* **1992**, *69*, 3397−3400.

(30) O'Day, P. A.; Rehr, J. J.; Zabinsky, S. I.; Brown, G. E., Jr. *J. Am. Chem. Soc.* **1994**, *116*, 2938−2949.

tion number of 0.5, since both of the Mn atoms would "see" each other at the same distance. More Mn–Mn interactions at the same distance would give multiples of 0.5 for the coordination number. In this work the Debye–Waller parameters were allowed to vary over a range comparable with those derived from synthetic multinuclear Mn compounds. The energy of the absorption edge (E_0) was varied in simulations to allow better phase matching to the experimental waves. The values of the average distance R_i, the numbers of scattering atoms N_i at distance R_i, the Debye–Waller factor σ^2, and the threshold energy E_0 were simultaneously fit with a nonlinear least-squares fitting program.[20,27,31]

The normalized error sum (Φ) used to verify the quality of the fits is given by the equation

$$\Phi = \sum_i^N \left(\frac{1}{s_i}\right)^2 [\chi^{\text{expt}}(k_i) - \chi^{\text{calc}}(k_i)]^2 \quad (2)$$

where N is the number of data points, and $\chi^{\text{expt}}(k_i)$ and $\chi^{\text{calc}}(k_i)$ are the experimental and calculated EXAFS. The normalization factor s_i is defined as

$$\frac{1}{s_i} = k_i^3 / \sum_j^N k_j^3 |\chi_j^{\text{expt}}(k_j)| \quad (3)$$

The ϵ^2 error accounts for the number of variable fit parameters (p), and the number of independent data points (N_{ind}) is estimated to be equal to $2\Delta k \Delta R/\pi$, where Δk is the k range of the data used and ΔR is the width of the Fourier-filtered peak.[32,33]

$$\epsilon^2 = [N_{\text{ind}}/(N_{\text{ind}} - p)]N^{-1}\Phi \quad (4)$$

A negative value of ϵ^2 indicates that the fit is underdetermined, and the fit solution is considered not unique. Generally, including more shells (which increases the value of p) results in a decrease in Φ. The ϵ^2 value therefore indicates whether fits were under- or overdetermined and whether the quality of fit is improved upon inclusion of extra shells.

Results

Synchronization of the S State Formation. The PS II samples were treated with PPBQ and given two preflashes to prevent loss of the S_2 and S_3 states by two processes of recombination. One path is decay of the S_2 and S_3 states to the S_1 state by recombination with the electrons from plastoquinone Q_B^-.[34,35] In the presence of exogenous electron acceptor PPBQ, the half-time for the S_2 and S_3 state recombinations increased to ~3.5 min.[36] The flash interval in our experiment was typically 1.5 s, and the PS II samples were frozen within 1 s in liquid nitrogen after the last flash. In the presence of PPBQ, the loss of S_2 and S_3 owing to recombination after one or two flashes was therefore negligible.

A second path for S_2 and S_3 state loss is through fast recombination with reduced Y_D in the dark.[37–40] Because these dark recombination reactions happen in seconds, the interval between the Xe lamp or Nd:YAG laser flashes (~1.5 s) in our experiments cannot be ignored. The preflash treatment oxidizes most of the Y_D to Y_D^{ox}, as shown by a 30–50% increase in the

amplitude of the Y_D^{ox} EPR signal.[16] Therefore, the PS II centers are synchronized to the $S_1Y_D^{\text{ox}}$ state before the samples receive the subsequent flashes, thus minimizing Y_D recombination with higher S states. The application of 0–5 flashes after the preflash protocol did not lead to a further increase of the Y_D^{ox} signal, indicating that, at that point, the recombination between reduced Y_D and the higher S states did not occur to any significant extent.

Extraction of S_3 EXAFS. Sets of PS II samples were synchronized in the S_1 state before being given a series of 0–5 flashes. The S_2 multiline EPR signal (MLS), generated after one flash, oscillates with a period of four, and can thus be used to precisely quantitate the S state distribution for each flash number. The actual S state distributions in samples given a particular number of flashes were obtained from the best fit of the flash-induced multiline EPR signal (MLS) oscillation pattern to the Kok model.[6] The first flash induced the maximal amount of MLS. The MLS oscillation pattern exhibits a periodicity of four, with maxima after the first and fifth flash, as expected.[41]

Assuming that after the preflash protocol the samples have a 100% S_1 population, the Kok model cast in terms of only two parameters (misses and double hits) describes the damped period-four MLS oscillation well. The best fit was found with 12% misses and 5% double hits for Xe flash lamp illumination and 14% misses and 0% double hits when a Nd:YAG laser was used for flash illumination.[16] Using these fit values, the S state distributions in samples given two flashes was calculated. This *independent* information on the S state distributions allows us to extract reliably the EXAFS spectra of the *pure* S_3 state from the experimentally acquired spectra of samples given two flashes. The best fit to the MLS oscillation pattern usually led to ~70% (for the Xe flash lamp illumination) and ~75% (for laser flash illumination) yield of the S_3 state after two flashes. In samples given two Xe lamp flashes the composition was 8% S_0, 2% S_1, 20% S_2, and 70% S_3, and from the Nd:YAG laser the composition was 0% S_0, 2% S_1, 24% S_2, and 74% S_3. The S_0 contribution was neglected for samples made using Xe flash lamp illumination. Because the EXAFS spectra of S_1 and S_2 states are nearly identical,[11] we used either 22% (Xe flash) or 26% (YAG laser) S_2 spectra. The S_2 state spectrum used for subtractions was obtained using a concentrated sample that was continuously illuminated at 190 K to produce the S_2 state characterized by the multiline EPR signal. This protocol was followed to minimize the contribution of noise that is introduced as a consequence of subtraction procedures. There were no discernible differences in the S_3 state spectra obtained by the two flash protocols.

The S_2 state contribution to the spectrum of a sample given two flashes, determined using MLS data as described above, was subtracted from the total spectrum and renormalized to yield the S_3 state EXAFS spectrum. There are no significant differences in the EXAFS spectra generated by subtraction in E-space or k-space. We present only the S_3 spectra generated by using the raw k-space data. Fourier transformation and isolation of individual Fourier peaks for the S_3 state was carried out on EXAFS spectra calculated using raw k-space data generated as described above.

Nine independent S_3 spectra collected from five X-ray runs were constructed and are presented as six data sets (S_3A–F) in

(31) Goodin, D. B. Lawrence Berkeley Laboratory Report LBL-16901 Thesis, University of California, Berkeley, 1983.

(32) Bunker, G. A.; Hasnain, S. S.; Sayers, D. E. In *X-ray Absorption Fine Structure*; Hasnain, S. S., Ed.; Ellis Horwood: New York, 1991; pp 751–770.

(33) Binsted, N.; Strange, R. W.; Hasnain, S. S. *Biochemistry* **1992**, *31*, 12117–12125.

(34) Rutherford, A. W.; Crofts, A. R.; Inoue, Y. *Biochim. Biophys. Acta* **1982**, *682*, 457–465.

(35) Lavergne, J.; Étienne, A.-L. In *Photosynthesis III*; Akoyunoglou, G., Ed.; Balaban International Science Services: Philadelphia, PA, 1981; pp 939–948.

(36) Styring, S.; Rutherford, A. W. *Biochemistry* **1988**, *27*, 4915–4923.

(37) Babcock, G. T.; Sauer, K. *Biochim. Biophys. Acta* **1973**, *325*, 483–503.

(38) Velthuys, B. R.; Visser, J. W. M. *FEBS Lett.* **1975**, *55*, 109–112.

(39) Vermaas, W. E. J.; Renger, G.; Dohnt, G. *Biochim. Biophys. Acta* **1984**, *764*, 194–202.

(40) Styring, S.; Rutherford, A. W. *Biochemistry* **1987**, *26*, 2401–2405.

(41) Kok, B.; Joliot, P. In *Bioenergetics of Photosynthesis*; Govindjee, Ed.; Academic Press: New York, 1975; pp 387–412.
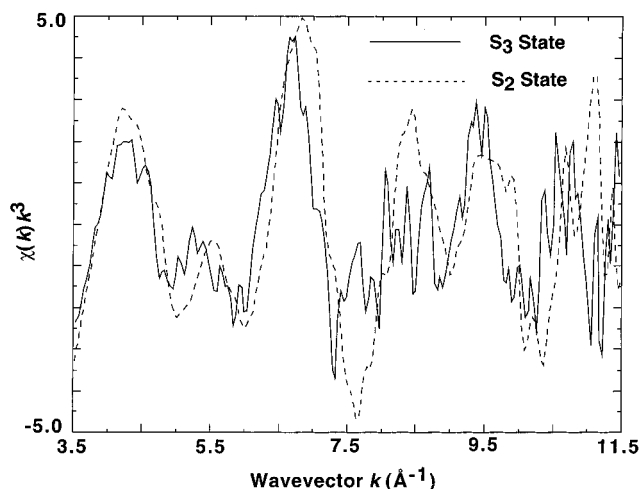
Figure 1. Background-subtracted k-space EXAFS data from S_2 (dashed line) and S_3 (solid line) states of PS II samples. The S_3 state spectrum was calculated from the spectrum obtained from a sample illuminated by two flashes by subtracting the residual S_2 state contribution. The amount of S_2 spectrum subtracted was determined by quantitating the amount of multiline EPR signal in samples given two flashes. The details of the quantitation are described in the Results section. These data have been multiplied by k^3. Differences in the phase and frequency of the EXAFS modulations and in the amplitude extend over the entire range of the spectra.

this report. Each of S_3A, S_3B, and S_3C was the average of two S_3 sample spectra.

EXAFS of the S_3 State. The k^3-weighted EXAFS spectra of representative S_3 and S_2 states are presented in Figure 1. Relative to the S_2 state, the spectra of the S_3 state samples show an overall difference in phase and amplitude within the data range of 3.5 to 11.5 Å^{-1}. We have previously observed changes in the modulations in the S_2 $g = 4.1$ and annealed ammonia-treated S_2 state samples.[42,43] In both cases, a Mn−Mn distance increase in one of the two di-μ-oxo dimanganese units was observed. Figure 1 clearly shows that there is an increase in the frequency of the oscillations in the S_3 state compared to the S_2 state as shown by the progressive change in phase of the oscillations toward higher k values between the two states. This result is indicative of an increase in distance for one or more of the scattering interactions. Figure 2 shows the Fourier-filtered back-transform of peaks I, II, and III (0−4 Å) of Figure 3 for the S_3 and S_2 states, where the differences in phase and amplitude between the two states are clearly evident. Interestingly, the EXAFS spectrum from a sample given two flashes is very similar to the calculated S_3 spectrum shown in Figure 1 (data not shown). This is not surprising because the two-flash sample is predominantly S_3 in composition (70−75%). However, this is important as it shows that subtraction used to generate the pure S_3 state spectrum does not introduce artifacts into the data.

Fourier transforms (FTs) of EXAFS data for pure S_2 and S_3 states are shown in Figure 3. The positions of the three peaks labeled I−III correspond to the shells of scatterers at different "apparent" distances from the Mn absorbers. These apparent distances, R', are shorter than the actual distances, R, due to an average phase shift induced by the potential of the given absorber−scatterer pair on the photoelectron.

In the S_2 state, peak I has been assigned to two N/O ligand atoms at a distance of ∼1.8 Å and ∼2−4 O/N ligand atoms at
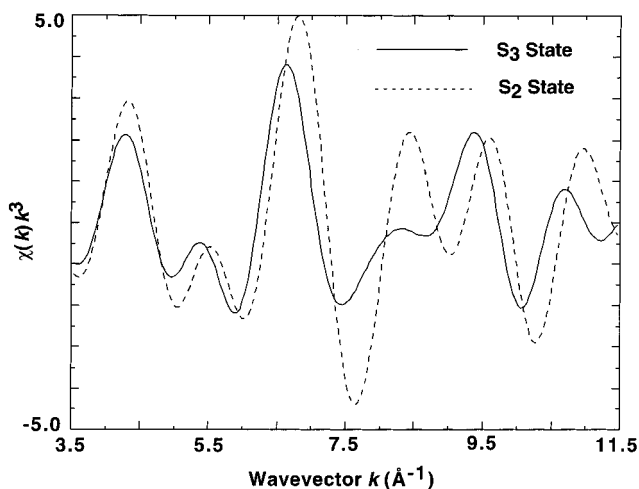
Figure 2. Fourier-filtered k-space EXAFS data from S_2 (dashed line) and S_3 (solid line) states of PS II samples (see Figure 1 caption and text for details of calculation of the S_3 state EXAFS spectrum). The Fourier window extended over the three Fourier peaks labeled I, II, and III (0−4 Å) shown in Figure 3. The differences in phase, frequency, and amplitudes between the raw S_2 and S_3 state EXAFS spectra (Figure 1) become very obvious in these Fourier-filtered spectra, where the high-frequency noise has been removed.

distances between 1.95 and 2.15 Å. The main contribution to peak II is from the backscattering of 1.2 ± 0.2 Mn neighbors at 2.7 Å from the Mn absorber. Peak III has been assigned to contributions from both Mn and Ca backscatterers at about 3.3 and 3.4 Å, respectively.[10,26,44] Studies from other groups prefer the assignment of peak III to backscattering from Mn or Ca at 3.3 Å,[45] or from Ca at 3.7 Å.[46]

Presented in the lower part of Figure 3 are Fourier transforms from 0 to 10 Å. The data at $R' > 4$ Å are a measure of the noise in the data showing the quality of the data obtained for the S_2 and S_3 states. The FTs from the six S_3 data sets all show peaks I and II that are significantly smaller in amplitude than the corresponding peaks of the S_2 spectrum. For the S_3 state, the amplitude of peak II is consistently smaller than that of peak I in all of the data sets. The vertical lines in Figure 3 emphasize that peaks II and III of the S_3 spectra are shifted to longer distances compared to those observed in the S_2 data. This is more evident in the expanded Fourier transform from 0 to 4 Å shown in the upper part of Figure 3. The distance increase is consistent with the shorter period in the oscillation pattern observed in the k^3-weighted EXAFS spectra shown in Figure 1 and discussed above. Fits to the EXAFS equation (discussed below) confirm this as a lengthening of Mn−Mn distances. The pattern of FT peaks in all of the six S_3 data sets remains the same under various background-removal procedures (in k-space or energy-space) and are therefore unlikely to be affected by data-processing artifacts.

Interestingly, a small Fourier feature is observed between peaks I and II, indicated by an arrow in Figure 3. It is possible that this small shoulder is also present in the S_2 state but becomes more evident in the S_3 state because of the shift of peak II to a longer apparent distance. Recent XAS studies in our laboratory on oriented PS II membranes in the S_3 state show

(42) Liang, W.; Latimer, M. J.; Dau, H.; Roelofs, T. A.; Yachandra, V. K.; Sauer, K.; Klein, M. P. *Biochemistry* **1994**, *33*, 4923−4932.

(43) Dau, H.; Andrews, J. C.; Roelofs, T. A.; Latimer, M. J.; Liang, W.; Yachandra, V. K.; Sauer, K.; Klein, M. P. *Biochemistry* **1995**, *34*, 5274−5287.

(44) Cinco, R. M.; Robblee, J. H.; Rompel, A.; Fernandez, C.; Yachandra, V. K.; Sauer, K.; Klein, M. P. *J. Phys. Chem. B* **1998**, *102*, 8248−8256.

(45) Riggs-Gelasco, P. J.; Mei, R.; Ghanotakis, D. F.; Yocum, C. F.; Penner-Hahn, J. E. *J. Am. Chem. Soc.* **1996**, *118*, 2400−2410.

(46) MacLachlan, D. J.; Hallahan, B. J.; Ruffle, S. V.; Nugent, J. H. A.; Evans, M. C. W.; Strange, R. W.; Hasnain, S. S. *Biochem. J.* **1992**, *285*, 569−576.
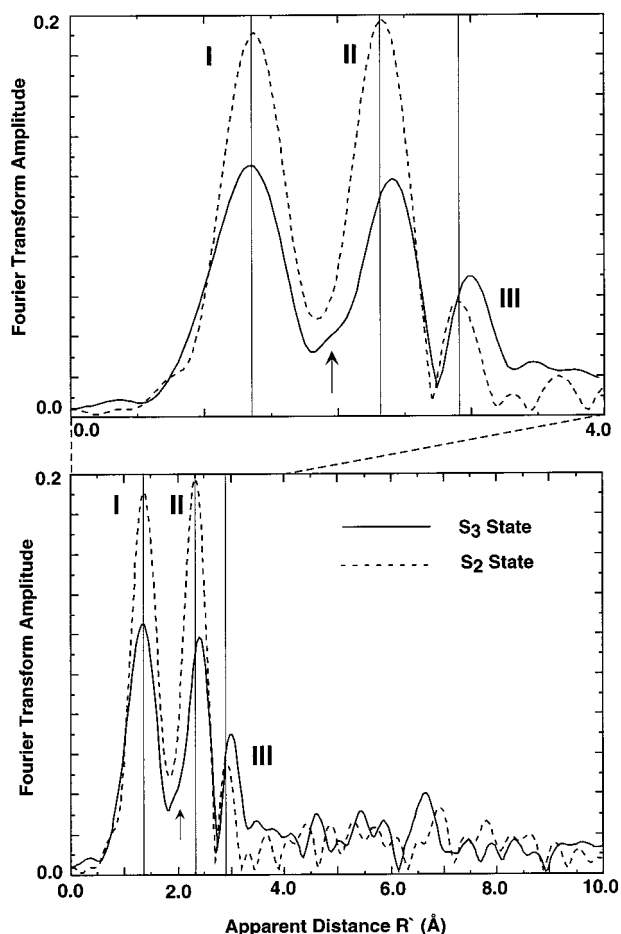
Figure 3. Fourier transform power spectra of S_2 (dashed line) and S_3 (solid line) states of PS II. The Fourier transform of the S_3 state was obtained from the calculated S_3 state EXAFS shown in Figure 1 (see text for details). The FTs are of the k^3-weighted EXAFS data from 3.5 to 11.5 Å^{-1} shown in Figure 1. The major Fourier peaks are labeled I, II, and III. The spectra are clearly different between the S_2 (dashed line) and S_3 states (solid line). The arrow points to a shoulder between peaks I and II at an apparent distance of 2.0 Å. There is a reduction in amplitude in all three peaks in the S_3 state compared to the S_2 state. More importantly, peaks II and III are at a greater apparent distance R′ for the S_3 state compared to the S_2 state as shown. The upper part of the figure shows an expanded version of the Fourier transform from 0 to 4 Å to show the differences in amplitude and apparent distance.

that this peak is also clearly present, that it is differently dichroic from peak II, and that it increases in amplitude when the **e**-vector of the X-rays is parallel to the membrane normal. Preliminary analysis suggests that this peak arises from a Mn−Cl interaction.[47] EXAFS spectra by Evans and co-workers of Ca-depleted samples prepared by NaCl treatment have also been modeled with a Cl contribution at ∼2.4 Å.[21] Recent studies have indicated that the presence of Cl is necessary only for the $S_2{\to}S_3$ and $S_3{\to}S_0$ transitions of the OEC, while the earlier steps of the cycle can proceed in its absence.[48,49]

The amplitude and distance changes of Fourier peak III in the S_3 state are less obvious. Peak III appears substantially above the noise level in three of the six S_3 FTs and is readily distinguishable from the noise in two others. Furthermore, all discernible third peaks in the data sets are shifted to a greater "apparent distance" than that observed in the S_2 spectrum.

(47) Fernandez, C.; Cinco, R. M.; Robblee, J. H.; Messinger, J.; Pizarro, S. A.; Sauer, K.; Yachandra, V. K.; Klein, M. P. In *Photosynthesis: Mechanisms and Effects*; Garab, G., Ed.; Kluwer Academic Publishers: Dordrecht, 1998; pp 1399−1402.

However, the amplitude of peak III is susceptible to noise components in the data, and the difference in the amplitude of this peak between the S_2 and S_3 spectra is harder to determine. Therefore, the changes of the amplitude of peak III in the S_3 spectra are less definite.

Curve Fitting of Mn EXAFS Data. Fourier isolation is commonly used to help simplify curve fitting of EXAFS data, allowing analysis of the contribution of single peaks. The isolation process, however, can introduce distortions in the extracted k-space data, especially at the start and end of the spectrum.[50] Closely spaced Fourier peaks can also be distorted if isolated individually. For analysis of the data presented here, Fourier peaks were isolated individually and in pairs to help simplify the spectra and to minimize the effects of distortions due to Fourier isolation.[51] Data sets from samples that allowed a clean isolation of the Fourier peaks of interest, I+II, II, II+III, or III, were used for fitting. Fourier peaks I and II were best isolated from samples A−D, peak II from samples B−F, peaks II and III from samples B−D, and peak III from samples A and D. Curve-fitting results of EXAFS data from representative S_3 and S_2 data sets (S_2 data from DeRose and co-workers[11] and Liang and co-workers[42]) are shown in Tables 1−4.

We were concerned about introducing artifacts because of the subtraction procedure used to generate the S_3 state EXAFS spectrum. To address this concern we performed fits on EXAFS data from a two-flash sample that is predominantly S_3 in composition. The data for 70−75% S_3-state composition are similar to those of the S_3 state spectrum. The fit parameters are also very similar to those reported below for the calculated pure S_3 state EXAFS data (data not shown).

Fourier Peaks I and II. Peaks I and II were isolated together and fit as a combination of two subshells (one Mn−O/N, one Mn−Mn) or four subshells (two Mn−O/N, two Mn−Mn) of scatterers. The corresponding parameters from the curve-fitting results are summarized in Table 1. Fitting results for the S_2 state agree well with our previous results on PS II samples.[10,11,42,43]

Results from curve-fitting peak I+II with two subshells indicate an increase in the Mn−Mn distance from 2.73 to ∼2.80 Å upon the $S_2 \to S_3$ transition. Furthermore, the Debye−Waller factor (σ^2) for the Mn−Mn shell is larger for the S_3 data. These results are reminiscent of our previous studies from the S_2 $g =$ 4.1 and the ammonium-treated S_2 samples; in both cases an amplitude reduction of peak II was observed and shown to result from a larger disorder in the Mn−Mn shell.[42,43]

For the Mn−O/N subshell, fits to peak I+II of the S_3 state resulted in a small change in the Mn−O/N distance relative to the S_2 sample, but larger Debye−Waller factors were required for the best fits. The results were suggestive of a more heterogeneous environment of these two subshells in the S_3 state (Table 1A). Best fits are obtained when two Mn−O/N subshells are included (Table 1B). There is little change between the S_2 and S_3 states in the Mn−O/N distances that are assigned to Mn-terminal ligands at ∼2.0 Å. However, there is a lengthening of the Mn−O/N subshell from 1.80 Å in the S_2 state to 1.86 Å in the S_3 state. The shorter 1.8 Å Mn−O distances are assigned to the Mn−O μ-oxo bridging ligands.

(48) Wincencjusz, H.; van Gorkom, H. J.; Yocum, C. F. *Biochemistry* **1997**, *36*, 3663−3670.

(49) Wincencjusz, H.; Yocum, C. F.; van Gorkom, H. J. *Biochemistry* **1999**, *38*, 3719−3725.

(50) Teo, B. K. *EXAFS: Basic Principles and Data Analysis*; Springer-Verlag: Berlin, 1986.

(51) Zhang, K.; Stern, E. A.; Ellis, F.; Sanders-Loehr, J.; Shiemke, A. K. *Biochemistry* **1988**, *27*, 7470−7479.

Table 1. Two-Shell and Four-Shell Simulations of Fourier Peak I and Peak II of the Native S_3 State Samples[a]

(A) Two-Shell Simulations

sample[b]	Mn−O/N interaction			Mn−Mn interaction			ΔE_0	Φ $(\times 10^3)^d$	ϵ^2 $(\times 10^5)^d$
	R (Å)	N	σ^2 (Å²)	R (Å)	N	σ^2 (Å²)			
S_3A	1.85	1.90	0.0060	2.78	0.81	0.0045	−17.23	1.38	1.46
S_3B	1.86	2.08	0.0083	2.80	0.92	0.0072	−14.22	1.56	1.15
S_3C	1.86	2.19	0.0098	2.82	0.97	0.0046	−9.98	1.38	0.94
S_3D	1.88	1.55	0.0065	2.79	1.23	0.0093	−14.09	1.43	2.10
$\langle S_3 \rangle$	1.86	1.93	0.0077	2.80	0.98	0.0064			
S_2 [e]	1.86	2.50	0.0050	2.73	1.10	0.0045			

(B) Four-Shell Simulations

sample[b]	two Mn−O/N interactions			two Mn−Mn interactions			ΔE_0	Φ $(\times 10^3)^d$	ϵ^2 $(\times 10^5)^d$
	R (Å)	N	σ^2 (Å²)	R (Å)	N	σ^2 (Å²)			
S_3A	1.85	1.50	0.0020^c	2.82	0.75	0.0020^c	−8.81	0.96	1.47
	2.02	0.94	0.0020^c	2.96	0.27	0.0020^c			
S_3B	1.85	1.34	0.0025	2.81	0.56	0.0030	−7.69	1.33	0.81
	2.01	0.77	0.0011	2.93	0.36	0.0043			
S_3C	1.87	1.56	0.0030	2.84	0.73	0.0015	−4.61	0.48	0.42
	2.05	1.09	0.0011	2.97	0.40	0.0087			
S_3D	1.86	0.82	0.0010	2.79	0.75	0.0028	−8.62	1.28	0.95
	1.99	0.76	0.0019	2.94	0.56	0.0037			
$\langle S_3 \rangle$	1.86	1.31	0.0021	2.82	0.70	0.0023			
	2.02	0.89	0.0015	2.95	0.40	0.0047			
S_2	1.80	1.40	0.0010	2.73	1.20	0.0025			
	1.98	0.80	0.0010						

[a] Fit parameters are defined in the text. Data are fit from $k = 3.5$ to 11.5 Å^{-1}. [b] Four individual S_3 data sets. [c] Parameter is fixed in the fit. [d] Quality of fit parameters Φ and ϵ^2 are defined in Materials and Methods. [e] The S_2 data sets are from refs 11 and 42. $\langle S_3 \rangle$ is the average of the individual fits presented. Three shell fits were also performed (see text for details).

Table 2. One-Shell and Two-Shell Simulations of Fourier Peak II of the Native S_3 State Samples[a]

(A) One-Shell Simulation

sample[b]	Mn−Mn interaction			ΔE_0 (eV)	Φ $(\times 10^3)^c$	ϵ^2 $(\times 10^5)^c$
	R (Å)	N	σ^2 (Å²)			
S_3B	2.85	1.27	0.0096	−5.67	0.30	0.50
S_3C	2.84	1.33	0.0067	−5.48	0.28	1.04
S_3D	2.80	1.29	0.0094	−12.05	0.39	1.17
S_3E	2.88	1.05	0.0058	−1.70	0.29	0.57
S_3F	2.87	1.14	0.0099	−2.69	0.68	0.55
$\langle S_3 \rangle$	2.85	1.22	0.0083			
S_2	2.73	1.20	0.0025			

(B) Two-Shell Simulation

sample[b]	Mn−Mn interaction			Mn−Mn interaction			ΔE_0 (eV)	Φ $(\times 10^3)^c$	ϵ^2 $(\times 10^5)^c$
	R (Å)	N	σ^2 (Å²)	R (Å)	N	σ^2 (Å²)			
S_3B	2.83	0.64	0.0021	2.97	0.47	0.0021	−3.04	0.13	0.54
S_3C	2.82	0.73	0.0010	2.96	0.55	0.0024	−2.24	0.12	0.11
S_3D	2.80	0.69	0.0018	2.95	0.62	0.0032	−5.30	0.22	0.65
S_3E	2.84	0.58	0.0022	2.95	0.53	0.0026	−0.71	0.23	0.27
S_3F	2.83	0.62	0.0046	2.97	0.58	0.0050	−0.64	0.30	0.34
$\langle S_3 \rangle$	2.82	0.65	0.0023	2.96	0.55	0.0031			
S_2	2.71	0.60	0.0010	2.81	0.60	0.0060			

[a] Fit parameters are defined in the text. Data are fit from $k = 3.5$ to 11.5 Å^{-1}. [b] Five individual S_3 data sets. [c] Quality of fit parameters Φ and ϵ^2 are defined in Materials and Methods. $\langle S_3 \rangle$ is the average of the individual fits presented. One Mn−Mn shell fit is better than a Mn−C fit by a factor of 3−4, and the two-shell Mn−Mn fits are better than one Mn−Mn and one Mn−C fits by a factor of 2−3 (see text for details).

To test whether an increase of heterogeneity in both peaks I and II could account for the amplitude reduction in the S_3 state, the data were also fit under the assumption that peak II contains two Mn−Mn subshells. As shown in Table 1B, this fit leads to a significant decrease of the normalized error sum (see Φ value, Table 1) in each of the S_3 samples. The best fits for peak II were found at distances of ~2.82 ($N = 0.56-0.75$) and 2.95 Å ($N = 0.27-0.56$) for the Mn−Mn shell. The fact that ϵ^2 remained positive after peaks I+II were fit with four subshells suggests that the fitting results were not underdetermined, because the number of free parameters does not exceed the number of independent data points. To test whether we have obtained a unique solution set at minimum Φ, we decreased number of the degrees of freedom by assuming the disorders for the individual subshells to be equal ($\sigma^2 = 0.002$ Å²). The unique solution under this assumption was found to be similar to those fits without restriction. One such fit is listed for sample

S_3A in Table 1. Peak I of the S_2 state was better fit with two subshells of N/O atoms at distances of 1.80 and 1.98 Å. Peak II of the S_2 state was also well fit with a single shell of 1.2 Mn at ~2.7 Å. An additional shell of Mn does not improve the overall fit quality of the S_2 sample (Table 1B).[11,42,43]

Three-shell fits were also performed that included two Mn−O/N distances and one Mn−Mn distance, or one Mn−O/N distance and two Mn−Mn distances (data not shown). When only one Mn−Mn distance is included, the Debye−Waller factors are large and the distance is ~2.85 Å, and when two Mn−Mn distances are included the Debye−Waller factors decrease and one can obtain fits with two distances at ~2.82 and 2.96 Å. The inclusion of one or two Mn−O/N shells has little bearing on the fits to the Mn−Mn distances. The results are not different from what is presently shown in the tables for two- and four-shell fits.

Table 3. Two-Shell and Four-Shell Simulations of Fourier Peaks II and III of the native S_3 State Samples[a]

(A) Mn–Mn Interaction Only

Two-Shell Simulation

sample[b]	Mn–Mn interaction R (Å)	N	σ^2 (Å²)	Mn–Mn interaction R (Å)	N	σ^2 (Å²)	ΔE_0 (eV)	Φ (×10³)[c]	ϵ^2 (×10⁵)[c]
S_3B	2.84	1.24	0.0095	3.39	0.33	0.0044	−6.04	0.28	0.39
S_3C	2.84	1.07	0.0048	3.43	0.61	0.0065	−6.17	0.52	0.35
S_3D	2.80	1.28	0.0094	3.39	0.93	0.0078	−9.82	0.37	0.33
$\langle S_3 \rangle$	2.83	1.20	0.0079	3.40	0.62	0.0062			
S_2	2.71	1.20	0.0025	3.34	0.30	0.0050			

Four-Shell Simulation

sample[b]	Mn–Mn interactions R (Å)	N	σ^2 (Å²)	Mn–Mn interactions R (Å)	N	σ^2 (Å²)	ΔE_0 (eV)	Φ (×10³)[c]	ϵ^2 (×10⁵)[c]
S_3B	2.82	0.72	0.0042	3.42	0.28	0.0043	−3.20	0.15	0.21
	2.96	0.55	0.0052	3.58	0.10	0.0090			
S_3C	2.83	0.73	0.0011	3.43	0.49	0.0056	−2.29	0.17	0.11
	2.96	0.55	0.0029	3.56	0.36	0.0018			
S_3D	2.80	0.68	0.0015	3.41	0.58	0.0024	−4.84	0.16	0.14
	2.95	0.61	0.0023	3.56	0.38	0.0034			
$\langle S_3 \rangle$	2.82	0.71	0.0022	3.42	0.45	0.0041			
	2.96	0.57	0.0035	3.57	0.28	0.0047			

(B) Mn–Mn and Mn–Ca Interactions

Two-Shell Simulation

sample[b]	Mn–Mn interaction R (Å)	N	σ^2 (Å²)	Mn–Ca interaction R (Å)	N	σ^2 (Å²)	ΔE_0 (eV)	Φ (x10³)[c]	ϵ^2 (x10⁵)[c]
S_3B	2.84	1.04	0.0082	3.45	0.43	0.0045	−6.65	0.21	0.17
S_3C	2.84	0.92	0.0040	3.51	0.63	0.0037	−5.61	0.52	0.42
S_3D	2.81	1.08	0.0070	3.44	1.07	0.0067	−9.70	0.48	0.42
$\langle S_3 \rangle$	2.83	1.01	0.0064	3.47	0.71	0.0050			
S_2	2.71	1.20	0.0025	3.39	0.40	0.0050			

Four-Shell Simulation

sample[b]	Mn–Mn interactions	R (Å)	N	σ^2 (Å²)	Mn–Mn and Mn–Ca interaction	R (Å)	N	σ^2 (Å²)	ΔE_0 (eV)	Φ (×10³)[c]	ϵ^2 (×10⁵)[c]
S_3B	Mn–Mn	2.83	0.70	0.0039	Mn–Mn	3.41	0.29	0.0045	−2.78	0.13	0.18
	Mn–Mn	2.96	0.56	0.0051	Mn–Ca	3.63	0.16	0.0066			
S_3C	Mn–Mn	2.83	0.73	0.0010	Mn–Mn	3.43	0.49	0.0052	−2.40	0.16	0.11
	Mn–Mn	2.96	0.55	0.0030	Mn–Ca	3.61	0.36	0.0011			
S_3D	Mn–Mn	2.80	0.68	0.0017	Mn–Mn	3.40	0.48	0.0021	−4.73	0.15	0.13
	Mn–Mn	2.95	0.61	0.0027	Mn–Ca	3.60	0.44	0.0026			
$\langle S_3 \rangle$	Mn–Mn	2.82	0.70	0.0022	Mn–Mn	3.41	0.42	0.0039			
	Mn–Mn	2.96	0.57	0.0036	Mn–Ca	3.61	0.32	0.0034			

[a] Fit parameters are defined in the text. Data are fit from $k = 3.5$ to 11.5 Å⁻¹. [b] Three individual S_3 data sets. [c] Quality of fit parameters Φ and ϵ^2 are defined in Materials and Methods. $\langle S_3 \rangle$ is the average of the individual fits presented.

Fourier Peak II. The isolates of Fourier peak II from the S_2 or S_3 states are shown in Figure 4. It is obvious that there is a significant difference in the contribution to this peak between the S_2 and S_3 states. The change in frequency of the modulations, as shown by the progressive change in phase toward higher values of k, and differences in the amplitude of the modulations are clearly evident. Fitting parameters for peak II alone for five S_3 data sets are given in Table 2. Fitting of this isolate using a single shell confirmed an elongation of the Mn–Mn distance to ~2.85 Å for the S_3 state relative to the S_2 state (2.73 Å). The Debye–Waller factors for the S_3 samples were larger than the values for S_2 samples, indicating a large disorder in peak II for the S_3 state. As shown in Table 2B, peak II was better fit with two Mn–Mn subshells at 2.82 ($N = 0.58$–0.73) and 2.96 Å ($N = 0.47$–0.62) for the S_3 state. We could force a two-distance fit for the S_2 state that yielded distances of 2.71 and 2.81 Å. However, the fits are physically unreasonable because the Debye–Waller factors for a one-shell fit increased for a two-shell fit.

We had shown for the S_2 state that the fit for peak II with at least two Mn–Mn interactions at 2.7 Å is better than that with Mn–C alone.[11] We used a similar approach for fitting the S_3 state data, and a similar conclusion was drawn. We compared C fits to Mn fits under very similar fit conditions, and the Mn–Mn fits are better by a factor of 3–4. We also compared the two Mn–Mn distance fits (at 2.82 and 2.96 Å) with one Mn–Mn and Mn–C interactions, and again in this case the fits with two Mn–Mn distances are better than those with one Mn–Mn and Mn–C interactions by a factor of 2–3 (data not shown).

Fourier Peaks II and III. Fitting parameters for Fourier peaks II and III, using two subshells or four subshells, are listed in Table 3. Fits were performed on three of the six pure S_3 data sets that showed a peak III that was substantially above the noise level in the FTs. In the top parts of Table 3A and B we consider a simple model of one Mn–Mn shell accounting for peak II and one Mn–Mn or Mn–Ca shell for peak III. Again, the fitting results indicate a larger Mn–Mn distance at ~2.82 Å, with a much larger Debye–Waller factor observed in two of the three S_3 data sets. Furthermore, the Mn–Mn or Mn–Ca interaction at ~3.3 Å also increases by ~0.06 (for a single Mn–Mn shell) or ~0.08 Å (for a single Mn–Ca shell).

The best fits for the S_3 state were obtained by including four subshells (bottoms of Table 3A and B). The normalized error sum for each data set decreased by a factor of 2–3, and the Debye–Waller factors were also smaller compared to the single-shell fits. Peak II was again better fit with two Mn–Mn

Table 4. Fit Parameters for Fourier Peak III of the Native S_3 State Samples[a]

	One-Shell Simulation					
	Mn–Mn interaction					
sample[b]	R (Å)	N	σ^2 (Å²)	ΔE_0 (eV)	Φ ($\times 10^3$)[c]	ϵ^2 ($\times 10^5$)[c]
S_3A	3.42	0.65	0.0056	−5.74	0.16	0.84
S_3D	3.41	0.82	0.0076	−6.93	0.39	0.21
$\langle S_3 \rangle$	3.42	0.74	0.0066			
S_2	3.36	0.30	0.0030			

	Two-Shell Simulation								
	Mn–Mn Interaction Only								
	Mn–Mn interaction			**Mn–Mn interaction**					
sample[b]	R (Å)	N	σ^2 (Å²)	R (Å)	N	σ^2 (Å²)	ΔE_0 (eV)	Φ ($\times 10^3$)[c]	ϵ^2 ($\times 10^5$)[c]
S_3A	3.43	0.52	0.0020[d]	3.58	0.23	0.0020[d]	−2.29	0.15	0.77
S_3D	3.41	0.57	0.0026	3.57	0.37	0.0031	−2.39	0.30	0.36
$\langle S_3 \rangle$	3.42	0.55	0.0023	3.58	0.30				

	Mn–Mn and Mn–Ca Interactions								
	Mn–Mn interaction			**Mn–Ca interaction**					
sample[b]	R (Å)	N	σ^2 (Å²)	R (Å)	N	σ^2 (Å²)	ΔE_0 (eV)	Φ ($\times 10^3$)[c]	ϵ^2 ($\times 10^5$)[c]
S_3A	3.43	0.48	0.0020[d]	3.64	0.27	0.0020[d]	−1.43	0.10	0.53
S_3D	3.40	0.48	0.0023	3.60	0.45	0.0026	−2.50	0.17	0.12
$\langle S_3 \rangle$	3.42	0.48	0.0020	3.62	0.36	0.0025			
S_2	3.38	0.30	0.0020	3.39	0.30	0.0070			

[a] Fit parameters are defined in the text. Data are fit from $k = 3.5$ to 11.5 Å⁻¹. [b] Five individual S_3 data sets. [c] Quality of fit parameters Φ and ϵ^2 are defined in Materials and Methods. [d] Parameter is fixed in the fit. $\langle S_3 \rangle$ is the average of the individual fits presented.
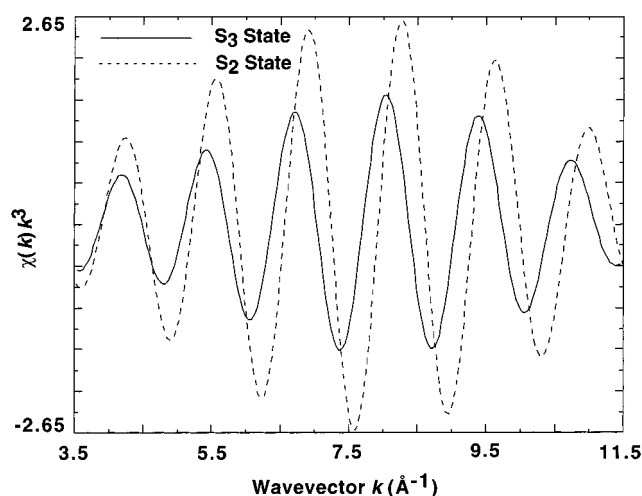
Figure 4. EXAFS contributions from Fourier peak II from S_2 (dashed line) and S_3 (solid line) states of PS II. The Fourier transform of the S_3 state was obtained from the calculated S_3 state EXAFS shown in Figure 1 (see text for details). Fourier peak II is assigned to Mn–Mn interactions at 2.7 Å in the S_1 and S_2 states. The increase in frequency evident in this figure in the S_3 state compared to that in the S_2 state is because of the increase in the Mn–Mn distance in the S_3 state. The $\sin(2kR + \alpha(k))$ contribution to the EXAFS (eq 1) dictates that an increase in R will be reflected in an increase in the frequency, as shown in the S_3 data compared to the S_2 state spectra. EXAFS techniques are most sensitive to such changes in frequency because the changes are manifest over the entire range of the spectra and hence less susceptible to contributions from noise in the spectra.

interactions at distances (2.82 and 2.96 Å) similar to the results from fitting peak I+II. Peak III can be fit reasonably well to two subshells of Mn–Mn (~3.42 and ~3.57 Å) or one Mn–Mn (~3.41 Å) plus one Mn–Ca interaction (~3.61 Å).

Fourier Peak III. Table 4 presents fitting parameters of peak III alone on data sets S_3A and S_3D. Fits with a single shell of Mn–Mn were worse than those with two subshells. Also, Mn–Mn fits are clearly better when compared to Mn–C fits. A higher degree of disorder was observed for the Mn–Mn fits, which suggested the need for an extra subshell. However, as

shown above, the Mn–Mn distance was longer relative to that in the S_2 state in the one-shell fits. Best fits were obtained in fits with two subshells in which one 3.62 Å Mn–Ca interaction was included. For fits of peak II+III or peak III only, the distance obtained from each subshell of the native S_3 state is consistently longer (0.04–0.23 Å) than those from the native S_2 state.
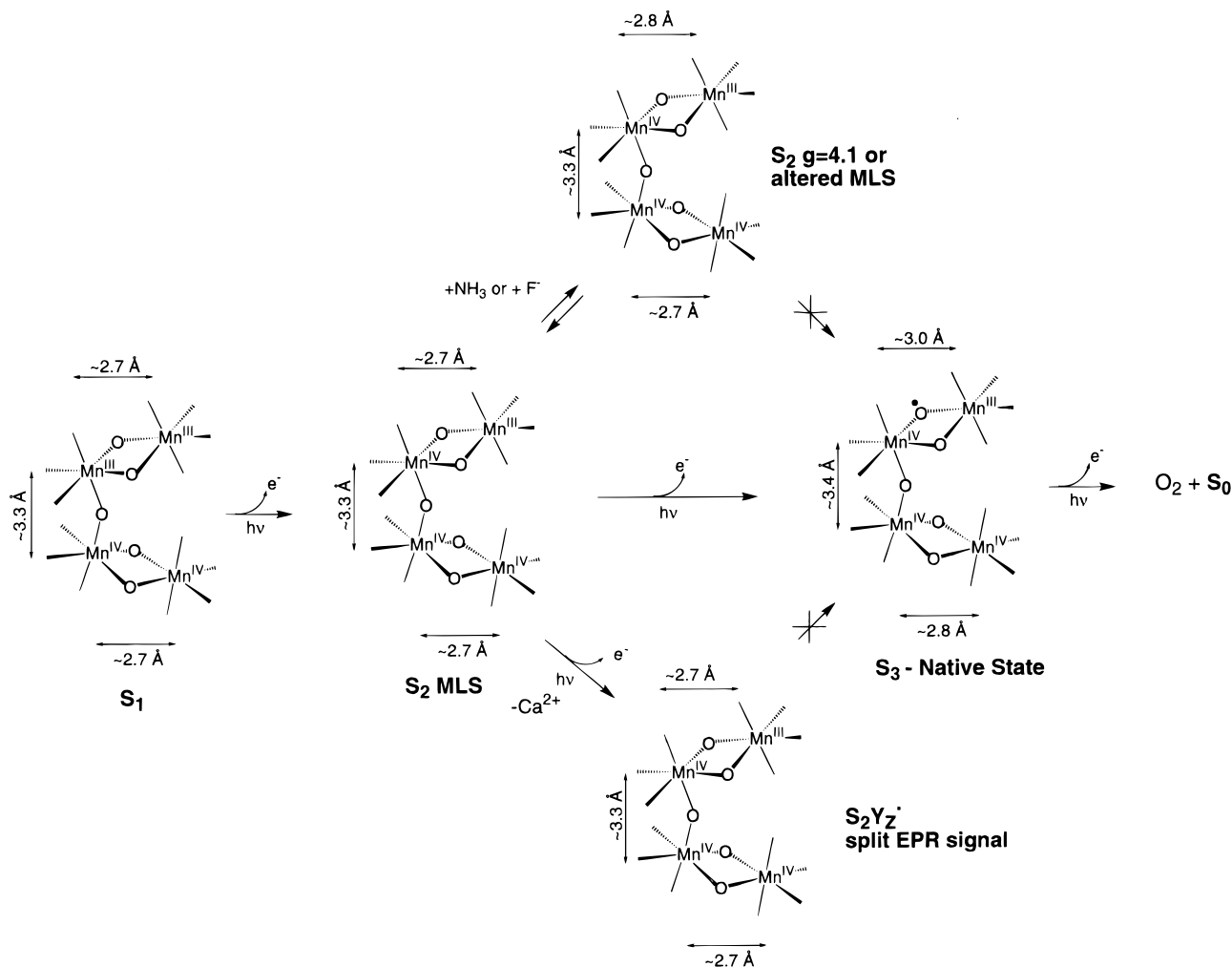
Fits to peak III alone are difficult for the S_3 samples. First, the quality of fits is poorer owing to the noise level in the data. Also, these samples are very dilute (~4–5 mg/mL of Chl) to guarantee a complete turnover by single laser or Xe lamp flash. In addition, the contribution from peak III is small compared with the total EXAFS, and multiple contributions from other low-Z elements are possible at longer distances from the absorber. Finally, distortions can arise by Fourier isolation of such a small feature, especially because it is near a much larger peak II. Considering the limitations, we chose to perform peak III simulations on the two best S_3 data sets. The fact that the fitting results are similar to those from peak II+III (Table 3) indicates the fitting parameters obtained are valid.

Discussion

Comparison of the Structure of Mn Cluster in the S_1, S_2, and S_3 States. By comparison with the structural motifs present in multinuclear Mn complexes (for details see refs 52 and 53, and refs 1b, 9, 43, and 44 in ref 5), we proposed that the Mn cluster in PS II consists of a pair of di-μ-oxo-bridged Mn binuclear clusters linked through a mono-μ-oxo bridge. The 2.7 Å Mn–Mn distance is characteristic of di-μ-oxo-bridged models, and the 3.3 Å Mn–Mn distance is characteristic of mono-μ-oxo-bridged Mn–Mn distances. The dimer-of-dimers model was proposed on consideration of the above data.[10] We described in a previous publication the various topological alternatives that are compatible with our EXAFS data,[11] and in this paper we discuss the structure of the Mn cluster in the S_3 state with the simplest of options that is compatible with our EXAFS data.

(52) Pecoraro, V. L. In *Manganese Redox Enzymes*; Pecoraro, V. L., Ed.; VCH Publishers: New York, 1992; pp 197–231.

(53) Wieghardt, K. *Angew. Chem., Int. Ed. Engl.* **1989**, *28*, 1153–1172.

~2.8 Å

S_2 g=4.1 or altered MLS

~3.3 Å

~2.7 Å

+NH₃ or + F⁻

~2.7 Å

~3.3 Å

~3.0 Å

~2.7 Å

~3.3 Å

e⁻
hv

e⁻
hv

~3.4 Å

e⁻
hv

O_2 + S_0

~2.7 Å

S_1

~2.7 Å

S_2 MLS

e⁻
hv

-Ca²⁺

~2.8 Å

S_3 - Native State

~2.7 Å

~3.3 Å

$S_2Y_Z^•$
split EPR signal

~2.7 Å

Figure 5. Summary of the changes in Mn−Mn distances in the native S_1, native S_2, modified S_2, S_3' ($S_2Y_Z^•$), and native S_3 states as determined by XAS. The increase in Mn−Mn distances in the S_3 state argues against the presence of di-μ-oxo bridges between Mn atoms. It is possible that the di-μ-oxo motif is unchanged in the other states presented in the schematic.

The changes in Mn−Mn distances occurring during the $S_1 \rightarrow S_2$ and $\rightarrow S_3$ transitions within the context of the dimer-of-dimer model described above is shown in Figure 5.

The first step in the scheme is the conversion of the dark, stable S_1 state to the S_2 state that is characterized by the multiline EPR signal. Little change is observed in the fitting parameters for Fourier peaks II and III when the Mn cluster undergoes this transition. This step involves a Mn-centered oxidation, as demonstrated by the appearance of the MLS during this transition and by our Mn K-edge and Mn Kβ emission studies.[16,54] Fourier peak II, corresponding to the averaged Mn−Mn distance in each di-μ-oxo dimanganese unit, is best fit to ~2.7 Å for both the S_1 and S_2 states.[11] EXAFS studies on oriented PS II in the S_1 and S_2 states show that there is heterogeneity in the 2.7 Å vectors, which suggests that these two binuclear species are not completely equivalent to each other.[55,56]

The inequivalence of the two di-μ-oxo-bridged Mn units becomes more evident in the S_2 state that is prepared by illumination at 130 K and characterized by the g = 4.1 EPR signal.[42] Similar results were obtained with NH₃-treated and annealed S_2 state samples[43] and in F⁻-treated samples.[57] The scheme in Figure 5 shows that there are paths from the MLS S_2 state that lead to two states, the S_2 g = 4.1 state inhibited by NH₃/F⁻ or the $S_2Y_Z^•$ states; neither of these states can proceed to the physiologically relevant S_3 state. These states are depicted in Figure 5 as branching away from the normal pathway leading to the S_3 state by photon absorption. However, the S_2 g = 4.1 state generated by 820 nm illumination at 130 K[58] can proceed to an S_3 state.[59] In the modified S_2 states, one of the Mn−Mn distances increases to ~2.85 Å, whereas there is very little change in the other 2.7 Å or the 3.3 Å Mn−Mn distance. With the degeneracy of the 2.7 Å distance lifted, we were able, by studying the dichroism of the Fourier peak, to assign the relative orientation of the 2.7 and 2.85 Å vectors.[43]

The NH₃-treated and F⁻-treated samples cannot advance beyond the modified S_2 state ($S_2Y_Z^•$ state). It is likely that F⁻

(54) Messinger, J.; Robblee, J. H.; Fernandez, C.; Cinco, R. M.; Visser, H.; Bergmann, U.; Glatzel, P.; Cramer, S. P.; Campbell, K. A.; Peloquin, J. M.; Britt, R. D.; Sauer, K.; Klein, M. P.; Yachandra, V. K. In *Photosynthesis: Mechanisms and Effects*; Garab, G., Ed.; Kluwer Academic Publishers: Dordrecht, 1998; pp 1279−1282.

(55) George, G. N.; Prince, R. C.; Frey, T. G.; Cramer, S. P. *Physica B* **1989**, *158*, 81−83.

(56) Mukerji, I.; Andrews, J. C.; DeRose, V. J.; Latimer, M. J.; Yachandra, V. K.; Sauer, K.; Klein, M. P. *Biochemistry* **1994**, *33*, 9712−9721.

(57) DeRose, V. J.; Latimer, M. J.; Zimmermann, J.-L.; Mukerji, I.; Yachandra, V. K.; Sauer, K.; Klein, M. P. *Chem. Phys.* **1995**, *194*, 443−459.

(58) Boussac, A.; Girerd, J.-J.; Rutherford, A. W. *Biochemistry* **1996**, *35*, 6984−6989.

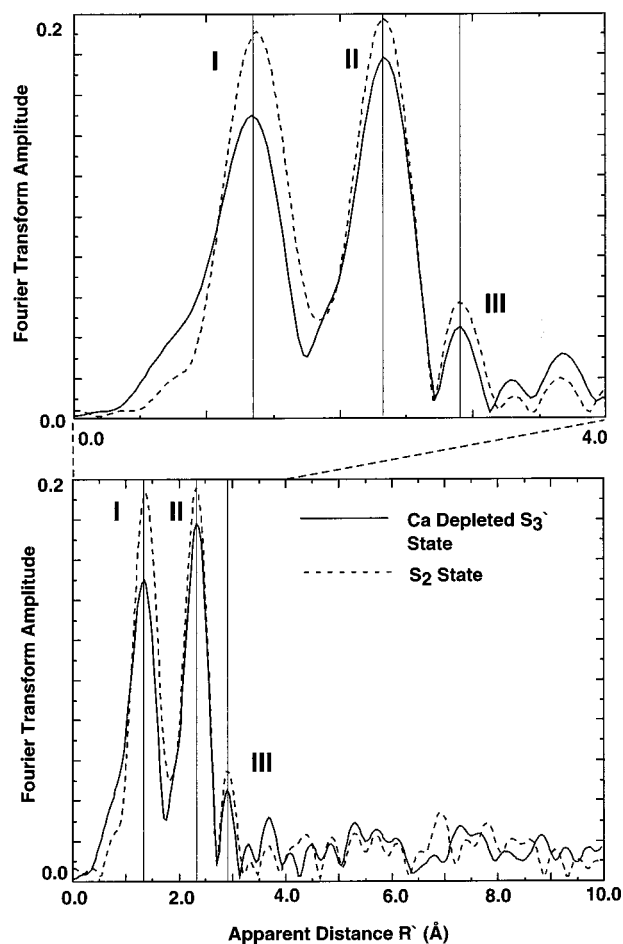(59) Zimmermann, J.-L.; Rutherford, A. W. *Biochemistry* **1986**, *25*, 4609−4615.

or NH_3 prevents the structural changes from occurring that are necessary for the formation of the S_3 state. In the case of NH_3, it is probably due to an amido group (NH_2^-) replacement of the oxo bridge involved in oxidation. The modification of the MLS spectra upon addition of NH_3 [60] and ESEEM studies using $^{14}NH_3$ and $^{15}NH_3$ demonstrated that NH_3 becomes a ligand of Mn.[61] The asymmetry parameter derived from ESEEM results suggested that the amido group is likely to be a bridging ligand.[61]

The other unproductive state generated from the S_2-MLS state is denoted in Figure 5 as the $S_2Y_Z^\bullet$ state generated in Ca-depleted samples. The Ca-depleted samples are inactive in O_2 evolution, while a broad $g = 2$ EPR signal has been observed in the "S_3' state" of such samples. In such samples the $g = 2$ broadened EPR signal has been confirmed to arise from the tyrosine Y_Z radical,[62,63] and it is proposed that the signal is broadened by interaction with the spin on the Mn cluster.[64]

We recently reported the XAS analysis from calcium-depleted S_3' state samples ($S_2Y_Z^\bullet$).[20] The position of peak II in the FT of S_3' state samples ($S_2Y_Z^\bullet$) was invariant relative to that of the native S_2 state sample (Figure 6). The EXAFS fits showed that the 2.7 Å Mn−Mn distances did not lengthen as observed in the native S_3 state samples and are essentially unchanged from those of the native S_2 state. This finding is surprising because the Mn K-edges from these calcium-depleted samples showed a behavior similar to that of the native PS II in that little or no shift was observed in the $S_2' \rightarrow S_3'$ (or $S_2Y_Z^\bullet$) transition. This difference between the native S_3 and calcium-depleted S_3' states indicates that the core di-μ-oxo-bridged structure is probably dissimilar in the native S_3 and the S_3' ($S_2Y_Z^\bullet$) states, with the structure in the $S_2Y_Z^\bullet$ state resembling the native S_2 state structure. It is reasonable to question how the transfer of one electron from the Mn cluster to Y_Z results in major changes in the Mn−Mn distances, as is observed in the native S_3 state. The roles of the Tyr_z and the Mn cluster in the process of water oxidation are clearly delineated by the comparison of the S_3 and the S_3' (or $S_2Y_Z^\bullet$) states. Instead of the Mn cluster just providing a scaffolding for water oxidation, this comparison shows that the structural change in the Mn cluster, initiated by the transfer of an electron from the Mn cluster to Tyr_z during the $S_2 \rightarrow S_3$ transition, might provide the trigger to the chemistry of the formation of the O−O bond. The results show that the Mn cluster is involved in a much more intimate manner in the catalysis than just providing the framework. The implications to the mechanism are significant (see below).

In Ca-depleted systems the tyrosine Y_Z radical is stabilized, and the oxidation of the Mn−OEC and the concomitant changes in Mn−Mn distances are prevented. In the S_3 state, with Ca present, the radical resides on the Mn cluster; however, in the absence of Ca, the radical resides on tyrosine Z. Thus, Ca is proposed to play a crucial role in controlling the redox potential and thus the course of the mechanism of water oxidation.

Earlier XAS data from the S_3 state samples produced by a cryogenic double-turnover method indicated increased disorder in the peak at 2.7 Å, indicative of the presence of two nonequivalent di-μ-oxo-bridged clusters in the S_3 state.[12] The principal result of that work was that a small but significant

(60) Beck, W. F.; de Paula, J. C.; Brudvig, G. W. *J. Am. Chem. Soc.* **1986**, *108*, 4018−4022.
(61) Britt, R. D.; Zimmermann, J.-L.; Sauer, K.; Klein, M. P. *J. Am. Chem. Soc.* **1989**, *111*, 3522−3532.
(62) Gilchrist, M. L., Jr.; Ball, J. A.; Randall, D. W.; Britt, R. D. *Proc. Natl. Acad. Sci. U.S.A.* **1995**, *92*, 9545−9549.
(63) Peloquin, J. M.; Campbell, K. A.; Brit, R. D. *J. Am. Chem. Soc.* **1998**, *120*, 6840−6841.
(64) Lakshmi, K. V.; Eaton, S. S.; Eaton, G. R.; Frank, H. A.; Brudvig, G. W. *J. Phys. Chem. B* **1998**, *102*, 8327−8335.

Figure 6. Fourier transform power spectra of S_2 (dashed line) and Ca-depleted S_3' or $S_2Y_Z^\bullet$ (solid line) states of PS II.[20] The FTs are of k^3-weighted EXAFS data from 3.5 to 11.5 Å^{-1}. There is a small difference in amplitudes, but there is no shift in apparent distance, in marked contrast to the Fourier transforms shown in Figure 3. The expanded version from 0 to 4 Å shown in the upper part of the figure makes the lack of a shift obvious.

structural change was found to accompany the $S_2 \rightarrow S_3$ transition. Specifically, the second Fourier peak, representing Mn scatterers at about 2.7 Å, was decreased in amplitude by about 40−50% compared to the Fourier peak for the S_2 state and was better simulated by distances differing by $\sim$0.15 Å. We note that the S_3 state in that work was generated by cryogenic turnover at 240 K of chemically treated PS II. The earlier data were collected at 190 K using a single-element Si(Li) detector, and the S/N was poor compared to that of our present data that were collected at 10 K using a 13-element Ge detector. The quality and smaller range of data, and the method of generation of the S_3 state, might be responsible for the differences. However, it was obvious even with the earlier data that a structural change that involved the lengthening of the Mn−Mn distance was occurring between the S_2 and S_3 states and was absent during the $S_1 \rightarrow S_2$ state transition.

The EXAFS results presented in this paper represent the first detailed analysis of data from native S_3 state samples created under physiological conditions with saturating actinic flash illumination (preliminary results from our group, Liang and co-workers,[19] have appeared in conference proceedings). During the $S_2 \rightarrow S_3$ transition there is a significant change in the 2.7 Å Mn−Mn distances that characterize the di-μ-oxo-bridged Mn−Mn units. One of the main conclusions from this study is that there is an increase in both the short Mn−Mn distances from

3410   *J. Am. Chem. Soc., Vol. 122, No. 14, 2000*

Liang et al.

2.7 Å to ~2.8 and ~3.0 Å. The results for the native S_3 state are shown in the scheme in Figure 5.

The k^3-weighted EXAFS spectra of the native S_3 state show an overall amplitude reduction with the most pronounced difference in the region $k = 7.5-10$ Å^{-1}, and a distinct difference in the phase and frequency of the modulations (Figures 1, 2, and 4). The perturbation in the Mn−Mn distances is different from that observed in the modified S_2 states. Each of these altered S_2 states gives a two-shell Mn−Mn fit that is consistent with the alteration of one of the two di-μ-oxo-bridged Mn−Mn distances from ~2.72 to 2.85 Å. Unlike the case in the modified S_2 states, the position of peak II from the native S_3 state clearly shifts to a longer distance in the FTs.

Parameters from the best fits for peak II derived from isolates of peak II only, peak I+II, or peak II+III all converge to Mn−Mn distances of 2.82 and 2.95 Å. These results underscore the point that during the $S_2 \rightarrow S_3$ transition under physiological conditions, *both* of the di-μ-oxo-bridged Mn−Mn units undergo structural changes that lead to an increase in the Mn−Mn distance. The structural changes are different between the two units. One is probably similar to those observed for the modified S_2 states, with a final Mn−Mn separation of 2.82 Å. For the other unit, a more significant change is observed that results in the Mn−Mn distance increasing to ~3.0 Å. A similar change in one of the Mn−Mn distances from 2.7 to 3.0 Å was observed in samples that had been depleted of Ca by NaCl treatment.[21]

The best fits for the Mn−O/N shell in Table 1B also show interesting differences between the S_2 and S_3 states. The fits converge to a distance of 1.80 and 1.98 Å for the S_2 state and to 1.86 and 2.02 Å for the S_3 state. The shorter Mn−O distance is characteristic of Mn−O bridging distances, and it increases from 1.80 Å in the S_2 state to 1.86 Å in the S_3 state. This is a significant change, and it provides additional evidence for the involvement of the bridging oxygen atoms during the $S_2 \rightarrow S_3$ transition.

The results from isotropic S_3 samples are supported by polarized EXAFS studies on oriented PS II in the native S_3 state. The data confirm that the two di-μ-oxo-bridged Mn−Mn dimer units are not equivalent. The polarized EXAFS data are different from those observed in the S_2 state.[43,56] Fourier peak II of S_3 is dichroic and is readily resolved to Mn−Mn distances of ~2.8 and ~3.0 Å, each with its own distinct projection on the membrane normal.[47] Recently, Dau and co-workers have reported results on the oriented S_3 state, showing an increase in the amplitude of Fourier peak II that is interpreted as an increase in the number of 2.7 Å Mn−Mn interactions in the S_3 state.[65] However, an examination of their FTs shows that Fourier peak II occurs at a longer distance and is broader compared to that in the S_2 state.

EXAFS analyses of PS II samples depleted of calcium and reconstituted by either calcium or strontium favor a model in which both manganese and calcium scatterers contribute to peak III in the S_1 state.[26] More evidence for the proximity of calcium to the Mn cluster in the S_1 state has been obtained from Sr EXAFS studies.[44] In the present study of the S_3 state, it is seen that Fourier peak III occurs at a greater apparent distance than that of the S_2 state. Simulation of peak II+III and of peak III alone indicates a lengthening of the two Mn−Mn distances or the Mn−Mn and Mn−Ca distances compared to the S_2 state (Tables 3 and 4).

Implication to the Mechanism of Water Oxidation. Two essential factors are considered to construct possible structural arrangements of the Mn cluster in the S_3 state. First, our Mn K-edge inflection-point data better support the interpretation that Mn is not oxidized during the $S_2 \rightarrow S_3$ transition. These data are reinforced by our recent Mn Kβ emission studies of the various S states.[54] Second, the Mn−Mn distance in both of the di-μ-oxo-bridged units increases from 2.72 to 2.82 and 2.95 Å, respectively, upon the formation of the S_3 state. Furthermore, the Mn−Mn distance of 3.3 Å increases by 0.04 Å, and the Mn−Ca (or Mn−Mn) distance also increases by 0.2 Å during the $S_2 \rightarrow S_3$ transition (Table 4). These changes imply a significant structural change in the Mn cluster as it proceeds to the S_3 state. It is hard to rationalize such changes in Mn−Mn distances as arising purely from Mn oxidation. We propose that substrate/ water oxidation chemistry is occurring at this transition, leading to the significant structural changes. This hypothesis is supported by various experiments reported in the literature.

First, marked differences of about 10−20-fold have been observed in the efficiency of exogenous reductants such as NH$_2$-OH and NH$_2$NH$_2$ toward the S_2 and S_3 states, with S_3 being more resistant to reduction than S_2.[66] These large differences in reactivity between the S_2 and S_3 states have been interpreted as indicating that a significant structural change in electronic and nuclear geometry occurs during the $S_2 \rightarrow S_3$ transition, which is consistent with our proposal.

In addition, Renger and co-workers have shown in a series of experiments that the activation energies for the $S_1 \rightarrow S_2$ and $S_2 \rightarrow S_3$ transitions are markedly different in PS II preparations from a thermophilic cyanobacterium and from either PS II core or membrane fragments from spinach.[67−69] The activation energy increases by a factor of about 3 for $S_2 \rightarrow S_3$ compared to that for the $S_1 \rightarrow S_2$ transition. The authors attribute this marked difference in activation energy to the involvement of a significant structural change in the $S_2 \rightarrow S_3$ transition that is absent in the $S_1 \rightarrow S_2$ transition. Moreover, they have deduced an increase in the reorganization energy for the $S_2 \rightarrow S_3$ transition compared to that for the $S_1 \rightarrow S_2$ transition. Renger notes that these results are consistent with the assumption that a significant structural change accompanies the $S_2 \rightarrow S_3$ transition,[70] perhaps reflecting the onset of water oxidation chemistry.[71]

Protonation of oxo bridges in the S_3 state is another mechanism by which one can rationalize the lengthening of Mn−Mn distances. Successive protonation of di-μ-oxo bridges in synthetic binuclear Mn complexes has been shown to result in increases in the Mn−Mn distance successively from 2.7 to 2.8 and to 2.9 Å.[72,73] The distance increase seen for the S_3 state might be due to such protonation. However, it is generally agreed that deprotonation at the higher S states is more likely, and mechanisms based on deprotonation or H atom abstraction of the substrate, OH$^-$ or H$_2$O, linked to the tyrosine Z moiety have been proposed.[62,74,75]

(65) Dau, H.; Iuzzolino, L.; Dittmer, J.; Dörner, W.; Meyer-Klaucke, W. In *Photosynthesis: Mechanisms and Effects*; Garab, G., Ed.; Kluwer Academic Publishers: Dordrecht, 1998; pp 1327−1330.

(66) Messinger, J.; Wacker, U.; Renger, G. *Biochemistry* **1991**, *30*, 7852−7862.

(67) Renger, G.; Hanssum, B. *FEBS Lett.* **1992**, *299*, 28−32.

(68) Koike, H.; Inoue, Y.; Renger, G. *Biochim. Biophys. Acta* **1987**, *893*, 524−533.

(69) Karge, M.; Irrgang, K.-D.; Renger, G. *Biochemistry* **1997**, *36*, 8904−8913.

(70) Renger, G. *Physiol. Plant.* **1997**, *100*, 828−841.

(71) Renger, G. *Photosynthetica* **1987**, *21*, 203−224.

(72) Baldwin, M. J.; Stemmler, T. L.; Riggs-Gelasco, P. J.; Kirk, M. L.; Penner-Hahn, J. E.; Pecoraro, V. L. *J. Am. Chem. Soc.* **1994**, *116*, 11349−11356.

(73) Larson, E. J.; Riggs, P. J.; Penner-Hahn, J. E.; Pecoraro, V. L. *J. Chem. Soc., Chem. Commun.* **1992**, 102−103.

(74) Hoganson, C. W.; Babcock, G. T. *Science* **1997**, *277*, 1953−1956.

(75) Randall, D. W.; Sturgeon, B. E.; Ball, J. A.; Lorigan, G. A.; Chan, M. K.; Klein, M. P.; Armstrong, W. H.; Britt, R. D. *J. Am. Chem. Soc.* **1995**, *117*, 11780−11789.

Alternatively, it has been proposed that formation of peroxide might follow protonation of a bridging μ-oxo ligand in the S_3 state and subsequent release of a dioxygen molecule.[76,77] Whether a peroxo-bridged Mn structure forms in the S_3 state is still under debate. The Mn–Mn distance in peroxo-bridged complexes is likely to be greater than 3 Å, assuming that the peroxo group replaces one of the di-μ-oxo bridges. Another option would be for the peroxo bridge to form between the two di-μ-oxo units. Calculations based on density functional theory support a structural arrangement in which the peroxo bridge forms between Mn atoms with accessible ferromagnetic states, as is the case for the Mn atoms that are linked by the mono-μ-oxo bridge.[78] Replacement of both of the di-μ-oxo bridges in one binuclear unit with a peroxo bridge results in a reduction of Mn. This arrangement is considered less likely because the Mn XANES spectra do not support such a reduction during the $S_2{\rightarrow}S_3$ transition.[16]

However, Renger has proposed that there could be equilibration between two species: one in which there is peroxide bond formation between two Mn(III) species, and one involving two Mn(IV) species with bound hydroxide or water.[70] Such a scenario would lead to no net change in Mn oxidation state and would be compatible with the Mn K-edge and Kβ emission results observed by our group.[16,54]

In addition to oxo-bridging ligands, Mn-terminal oxo ligands have also been proposed to be involved in dioxygen formation.[79,80] It has been proposed that Mn is ligated to activated O (Mn=O) produced by the abstraction of protons from Mn-bound water by a nearby tyrosine,[62,74,81] and the O–O bond is proposed to form between the oxo ligands of two adjacent Mn atoms.[82] However, it is hard to understand how changes in terminal ligation can generate such a profound change on the Mn–Mn distances in the S_3 state as reported here. Replacement of terminal ligands in di-μ-oxo-bridged model compounds has a minimal effect on the Mn–Mn distance of 2.7 Å that is characteristic of such di-μ-oxo-bridged Mn compounds.[53,83]

Limburg and co-workers[84] have recently reported a di-μ-oxo Mn complex that oxidizes water. They proposed that the O–O bond formation can be explained by a nucleophilic attack of a Mn=O or Mn–O radical species on a OH⁻ or H_2O that is either free or ligated to another Mn atom. On the basis of the Mn K-edge and EXAFS results, it is less likely that a Mn=O exists at the S_3 state of the OEC. However, a radical species is supported by the lack of any significant shift in the Mn K-edge inflection point energy and also by the Mn Kβ emission studies.[54]

The case for the involvement of the bridging oxygen atoms during the $S_2{\rightarrow}S_3$ transition and in the mechanism of oxygen evolution is manifold. It is easy to rationalize increases in Mn–Mn distances as being due to changes in the bridging structure. As described above, the Mn–O bridging distances increase from 1.80 to 1.86 Å during the $S_2{\rightarrow}S_3$ transition. NH_3, an inhibitor

of water oxidation and an analogue of the substrate/water, has been shown by ESEEM studies[61] to be coordinated to Mn, probably in a bridging position. XAS studies showed that one of the 2.7 Å Mn–Mn vectors is perturbed in NH_3-treated samples, with the distance increasing to 2.85 Å, an increase easily rationalized if an amido group were replacing an oxo group. Replacing a terminal O/N ligand with an NH_3 ligand cannot easily justify such an increase in the Mn–Mn distance.

We proposed earlier a model for the S_3 state in which an oxyl radical is generated on one of the μ-oxo bridges, which results in an increase of one of the Mn–Mn distances to ∼2.95 Å (Figure 7). Consistent with our XANES results, this structure implies that the oxidative equivalent is not stored on the Mn atoms per se during the $S_2{\rightarrow}S_3$ transition but is delocalized with significant charge and spin density on the bridging oxo ligand. Junge and co-workers have proposed a mechanism in which Mn is oxidized during the $S_0{\rightarrow}S_1$ and $S_1{\rightarrow}S_2$ transitions but involves the oxidation of bound substrate, OH⁻, to a hydroxide radical during the $S_2{\rightarrow}S_3$ transition, with a small fraction already present as a peroxide intermediate.[85,86]

The presence of an unpaired electron on the oxygen changes the spin state of the Mn complex; therefore, the MLS signal disappears, as observed from the results of EPR spectroscopy. Parallel-mode EPR studies by Matsukawa and co-workers have shown the presence of EPR resonances at $g = 12$ and 8 that are best simulated by an $S = 1$ excited-state spin species in the S_3 state.[87] The authors rationalize these results as arising from a coupling between the $S = {}^1/_2$ complex, characterized by the MLS EPR signal, interacting with an $S = {}^1/_2$ radical produced during the S_3 transition that leads to the disappearance of the MLS and generation of an integer spin state.

Siegbahn and Crabtree have proposed a new mechanism on the basis of quantum chemical studies where they have tried to reconcile the various biophysical data.[88] Spin-state considerations led them to propose a Mn–O oxyl intermediate in the S_3 state, with radical character on the terminal oxygen ligand, with the formation of the O–O bond proposed to occur between the oxyl radical and an outer-sphere water molecule. Recent calculations by Siegbahn have produced an energy minimum for the formation of the oxyl radical on the bridging O atom.[89] The Siegbahn and Crabtree mechanism involves only one Mn in the oxidation process and involves a radical species in the S_3 state, as proposed by our group.

We propose that the O–Mn–O angle in one of the di-μ-oxo-bridged Mn–Mn cores decreases in the S_3 state and, as a consequence, draws the two bridging oxo ligands closer for the imminent formation of an O–O bond before O_2 release. Consequently, the distance between the two Mn atoms lengthens. We previously proposed that in the S_4 state a dioxyl radical is produced which spontaneously converts to a peroxo species with the formation of an O–O bond (Figure 7).[5] This proposal results from the study of a synthetic inorganic di-μ-oxo-bridged di-Cu compound that has been shown to convert into an isomer with the formation of an O–O bond between the two bridged oxygens.[90] Alternatively, the formation of the oxyl radical on one dimer in the S_3 state and its reaction with OH⁻ or H_2O either on the other Mn dimer or in the outer sphere during the

(76) Baldwin, M. J.; Gelasco, P. J.; Pecoraro, V. L. *Photosynth. Res.* **1993**, *38*, 303−308.

(77) Pecoraro, V. L.; Baldwin, M. J.; Gelasco, A. *Chem. Rev.* **1994**, *94*, 807−826.

(78) McGrady, J. E.; Stranger, R. *Inorg. Chem.* **1999**, *38*, 550−558.

(79) Rüttinger, W.; Dismukes, G. C. *Chem. Rev.* **1997**, *97*, 1−24.

(80) Messinger, J.; Badger, M.; Wydrzynski, T. *Proc. Natl. Acad. Sci. U.S.A.* **1995**, *92*, 3209−3213.

(81) Pecoraro, V. L.; Baldwin, M. J.; Caudle, M. T.; Hsieh, W.; Law, N. A. *Pure Appl. Chem.* **1998**, *70*, 925-.

(82) Tommos, C.; Babcock, G. T. *Acc. Chem. Res.* **1998**, *31*, 18−25.

(83) *Manganese Redox Enzymes*; Pecoraro, V. L., Ed.; VCH Publishers: New York, 1992.

(84) Limburg, J.; Vrettos, J. S.; Liable-Sands, L. M.; Rheingold, A. L.; Crabtree, R. H.; Brudvig, G. W. *Science* **1999**, *283*, 524−527.
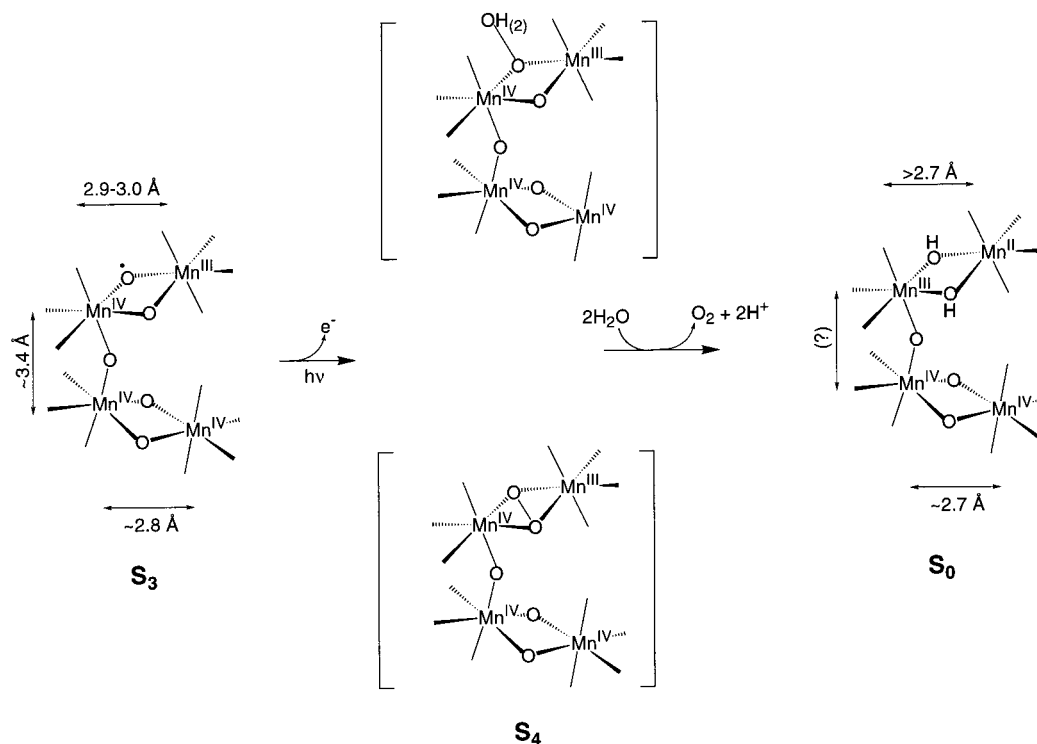
(85) Haumann, M.; Bögershausen, O.; Cherpanov, D. A.; Ahlbrink, R.; Junge, W. *Photosynth. Res.* **1997**, *51*, 193−208.

(86) Haumann, M.; Junge, W. *Biochim. Biophys. Acta* **1999**, *1411*, 86−91.

(87) Matsukawa, T.; Mino, H.; Yoneda, D.; Kawamori, A. *Biochemistry* **1999**, *38*, 4072−4077.

(88) Siegbahn, P. E. M.; Crabtree, R. H. *J. Am. Chem. Soc.* **1999**, *121*, 117−127.

(89) Siegbahn, P., personal communication.

Figure 7. Scheme showing the two different pathways by which an oxyl radical formed in the S_3 state could form an O−O bond in the transient S_4 state before release of dioxygen. One path involves the formation of an O−O bond between the two oxo groups of one binuclear unit. The other path for the formation of the O−O bond is the reaction of the oxyl radical formed with OH⁻ or H_2O that is a ligand of Mn or in the outer sphere of the Mn cluster. The Mn−Mn distances in the transient S_4 state are unknown at present.

subsequent S state conversion can lead to the formation of the O−O bond (Figure 7). The results reported by Messinger and co-workers support the presence of two nonequivalent exchangeable sites in the S_3 state as required by this proposal.[80,91]

Our proposed mechanism avoids the formation of the O−O bond until the most oxidized state (S_4) is reached. This precludes the formation and release of peroxide or other oxidation products of water in the earlier S states, thus preventing the system from "short circuiting" and avoiding the risk of damaging the polypeptides of Photosystem II.

Supporting Information Available: E-space S_3 state EXAFS spectrum; the data in *k*-space and the background that was removed to reduce the low-frequency contributions that show up as peaks at <1 Å in the Fourier transform; and the Fourier isolate of the *k*-space S_3 spectrum, shown overplotted on the S_3 EXAFS spectrum (PDF). This material is available free of charge via the Internet at http://pubs.acs.org.

(90) Halfen, J. A.; Mahapatra, S.; Wilkinson, E. C.; Kaderli, S.; Young, V. G., Jr.; Que, L., Jr.; Zuberbuhler, A. D.; Tolman, W. B. *Science* **1996**, *277*, 1953−1956.

(91) Hillier, W.; Messinger, J.; Wydrzynski, T. *Biochemistry* **1998**, *37*, 16908−16914.

JA992501U